Geol. Mag. **155** (*7*), *2018*, *pp. 1542–1565.* © *Cambridge University Press 2017*
doi:10.1017/S0016756817000437

Geochronology, petrology and geochemistry of the Mesozoic Dashizhuzi granites and lamprophyre dykes in eastern Hebei – western Liaoning: implications for lithospheric evolution beneath the North China Craton

LE XIONG*, JUNHAO WEI, WENJIE SHI, LEBING FU, HUAN LI, HONGZHI ZHOU, JIAJIE CHEN & MENGTING CHEN

Faculty of Earth Resources, China University of Geosciences, Wuhan 430074, China

(*Received* 9 May 2016; *accepted* 25 April 2017; *first published online* 5 June 2017)

Abstract – Geochronological, elemental and isotopic data of the Dashizhuzi granites and lamprophyre dykes from the eastern Hebei – western Liaoning on the northern North China Craton (NCC) provide an insight into the nature of their magma sources and subcontinental lithospheric mantle. The Dashizhuzi granites have an emplacement age of 226 Ma. They have enriched lithospheric mantle type 1 (EM1-like) Sr–Nd isotopic compositions, and have distinctive features of high Na_2O and Sr and low Y with high Sr/Y and $(La/Yb)_N$ ratios. These characteristics show that the Dashizhuzi granites originated directly from melting of mafic lower crust composed of pre-existing ancient crustal and enriched mantle-derived juvenile crustal materials at normal continental crustal depth of 33–40 km. The lamprophyre dykes are dated at 167 Ma, and can be divided into two groups. The Group 1 dykes have variable Sr–Nd isotopic compositions and mid-ocean-ridge basalt (MORB-) like Th/U, Ba/Th and Ce/Pb ratios, whereas the Group 2 dykes have enriched Sr–Nd isotopic compositions and notable high Co, Cr, MgO and low Al_2O_3 characteristics. These distinctive features suggest that the Group 1 dykes were derived from a relatively fertile lithospheric mantle source (garnet-facies amphibole-bearing lherzolite) which has experienced variable degrees of asthenospheric mantle-derived melt–peridotite interaction prior to melting. However, the Group 2 dykes were derived from an ancient garnet-facies phlogopite and/or amphibole-bearing lherzolite lithospheric mantle. Thinning of the Early Mesozoic lithospheric mantle beneath the northern NCC is dominantly through melt–peridotite interaction and thermo-mechanical erosion prior to Middle Jurassic time. The chemical compositions have been modified at the bottom of the lithospheric mantle through melt–peridotite interaction processes.

Keywords: mafic dyke, adakitic rocks, Mesozoic period, lithospheric thinning, Yanshan fold belt

1. Introduction

Recent studies have shown pronounced changes in lithospheric thickness, thermal state and petrological and geochemical compositions of the lithospheric mantle from an old, thick and refractory lithosphere during Palaeozoic time to a juvenile, thin and fertile lithosphere during Cenozoic time beneath the eastern North China Craton (e.g. Ma, 1987; Lu *et al.* 1991; Griffin, O'Reilly & Ryan, 1992; Menzies, Fan & Zhang, 1993; Griffin *et al.* 1998; Menzies & Xu, 1998; Xu *et al.* 1998; Zheng & Lu, 1999; Liu *et al.* 2015). However, the timing and mechanism of this replacement or removal of lithosphere still remains controversial (e.g. Xu, 2001; Gao *et al.* 2002; Zhang *et al.* 2002; Chen, Jahn & Zhai, 2003; Liu *et al.* 2004, 2011; Niu, 2005; Xu *et al.* 2006*b*, 2009; Zhang *et al.* 2009a; Fu *et al.* 2012*a*; Xia *et al.* 2013). The debate on the beginning of replacement or removal of lithosphere is mainly focused on whether it was a rapid or a more protracted transformation process, with opinion divided between the late Carboniferous – Late Triassic, the Late Triassic and Jurassic – Early Cretaceous (Zhang *et al.* 2002; Chen, Jahn & Zhai, 2003; Liu *et al.* 2004; Xu *et al.* 2009; Zhang *et al.* 2009*a*; Fu *et al.* 2012*a*).

Mesozoic magmatism may be used as a 'window' to help resolve the above questions of timing and mechanism of lithospheric thinning (Ma *et al.* 2014*a*). Following the assembly of the Mongolian composite terranes with the NCC during middle–late Permian time (Xiao *et al.* 2003; Li, 2006; Windley *et al.* 2007), a number of Triassic magmatic rocks (alkaline, mafic-ultramafic, felsic magmas and mafic dykes) intruded into supercrustal rocks in the northern NCC. Formation of these magmas was considered to involve at least five components, including asthenospheric mantle, enriched or juvenile lithospheric mantle, and juvenile or ancient lower continental crust (LCC) materials (e.g. Wu, Jahn & Lin, 1997; Shao *et al.* 1999; Liu *et al.* 2002; Tian *et al.* 2007; Peng *et al.* 2008; Fu *et al.* 2012*a*; Yang *et al.* 2012; Wu *et al.* 2014; Ye *et al.* 2014). It is believed that the above enriched lithospheric mantle beneath the NCC was formed during Archean time and replaced or metasomatized during late Palaeoproterozoic time (Wu, Jahn & Lin, 1997;

*Author for correspondence: 601224101@qq.com

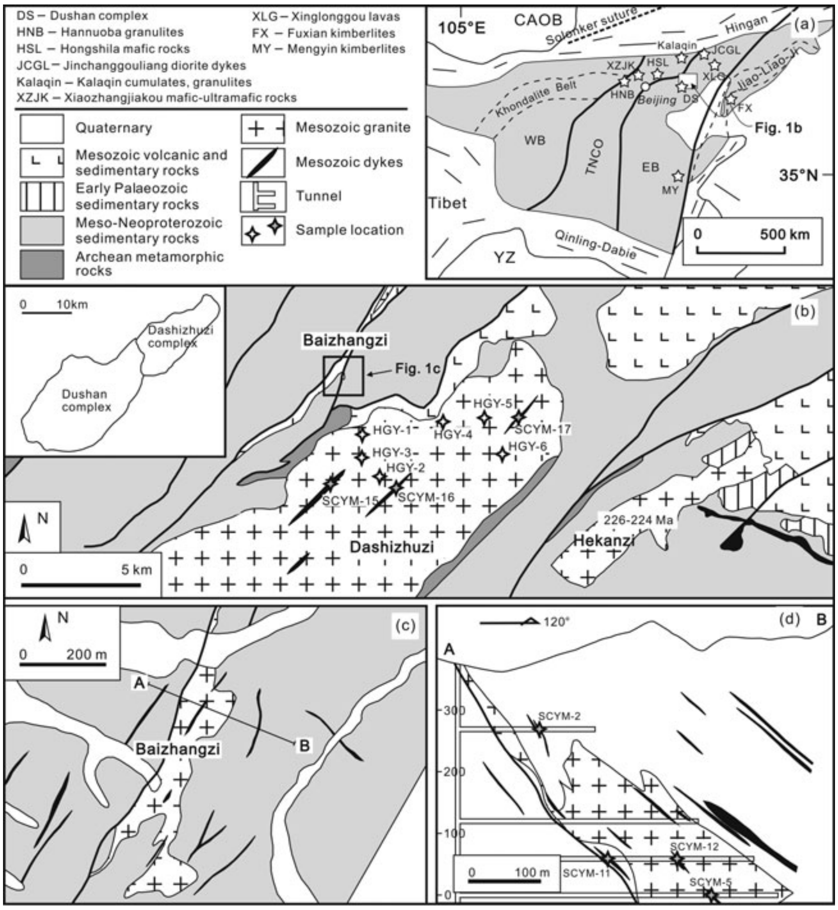

Figure 1. (a) Tectonic setting, modified after Gao *et al*. (2004) and Zhao *et al*. (2005), showing the location of (b). YZ – Yangtze craton; SC – South China Orogen; WB – Western Block of the North China Craton; EB – Eastern Block of the North China Craton; TNCO – Trans-North China Orogen; CAOB – Central Asian Oregenic Belt; Jiao-Liao-Ji – Jiao-Liao-Ji continental rift. (b) Simplified geological map of the eastern Hebei – western Liaoning area, showing the location of (c). The inset shows spatial correlations between the Dushan and the Dashizhuzi complexes. (c) Geological sketch map of the Baizhangzi area (modified after Team 109 of Metallurgy and Geology Exploration Company, Liaoning, 1990, unpub.), showing the location of cross-section A–B. (d) Profile of the Baizhangzi granites and lamprophyre dykes.

Gao *et al*. 2002; Wu *et al*. 2006*a*; Li *et al*. 2011; Liu *et al*. 2011, 2012, 2015); nevertheless, whether it was fertile or refractory remains under debate. This is vital for our understanding of the Phanerozoic lithospheric evolution beneath the NCC. Since Jurassic time another pronounced tectono-thermal event featured in the eastern NCC, accompanied by the emplacement of vast intrusive rocks and widespread volcanic rocks. Only a few studies have been carried out on mafic rocks formed at this time, however. Because igneous rocks often have deep crustal or mantle derivations, studies of such rocks can be a sufficient approach to understanding the nature of subcontinental lithosphere.

There are widespread Mesozoic mafic dykes distributed along the northern margin of the NCC (Shao & Zhang, 2002; Fu *et al*. 2010, 2012*a*; Zhang *et al*. 2010*a*; Zhang, Yuan & Wilde, 2014). They may provide efficient probes into the nature of the lower crust and lithospheric mantle given their instantaneous emplacement processes and minor resultant modifications. As important country rocks of the mafic dykes, only zircon U–Pb age and major- and trace-element data were reported for the granodiorites of the Dashizhuzi (DSZZ) complex that consists of granodiorites and granites (Ye *et al*. 2014). In this paper, we present zircon U–Pb ages, major- and trace-element data, and Sr–Nd isotope compositions for the lamprophyre dykes and the DSZZ granites exposed in the eastern Hebei – western Liaoning, and use these data to discuss their petrogenesis and implications for understanding their magma sources and the nature of the lithosphere beneath the NCC.

2. Geological setting

Containing continental rocks of age 3.85–3.2 Ga, the NCC was thought to be one of the oldest cratons in the world (Liu *et al*. 1992; Song *et al*. 1996; Zhai & Santosh, 2011). The NCC is composed of an Archean–Palaeoproterozoic metamorphosed basement overlain by Mesoproterozoic–Cenozoic cover. According to the lithological assemblages and geochemical, geochronological, structural and pressure–temperature (P–T) data, the basement of the NCC can be divided into the Eastern and Western blocks, separated by the Trans-North China Orogen (Fig. 1a; Zhao *et al*. 2001).

https://doi.org/10.1017/S0016756817000437 Published online by Cambridge University Press

Collision between the Eastern and Western blocks along the Trans-North China Orogen during late Palaeoproterozoic time led to the amalgamation of the NCC (Wu & Zhong, 1998; Zhao *et al.* 2001). The Eastern Block underwent Palaeoproterozoic rifting (Jiao-Liao-Ji continental rift) along its eastern margin before the collision of the Western and Eastern blocks (e.g. Li *et al.* 2005; Zhao *et al.* 2005). The craton was magmatically and tectonically quiescent until the occurrence of a tectono-thermal event at 0.98–0.60 Ga, recorded by some exposed Neoproterozoic mafic magmas and zircons in xenoliths derived from the lower crust (e.g. Shao, Zhang & Li, 2002; Zheng *et al.* 2012, 2013).

During Palaeozoic – early Mesozoic time, voluminous igneous rocks intruded into supercrustal rocks in the NCC. The eruption of Middle Ordovician kimberlites in Fuxian and Mengyin was followed by the uplift of the NCC, which resulted in the absence of Upper Ordovician – middle Carboniferous sedimentary rocks (Zheng *et al.* 2004*a*). During middle Carboniferous – Permian time, emplacement of voluminous granitic magmas in the northern part of the NCC was related to the complicated tectono-thermal processes of the Central Asian Oregenic Belt (CAOB; e.g. Xiao *et al.* 2003; Windley *et al.* 2007; Zhu, Yang & Wu, 2012). The Solonker suture in the CAOB marks the location of the final closure of the Palaeo-Asian Ocean and the collision between the NCC and the Mongolian composite terranes (Xiao *et al.* 2003) which led to significantly N–S-directed tectonic shortening of the continental crust in the northern NCC during middle–late Permian time (Zhang *et al.* 2011; Lin *et al.* 2013). From early Mesozoic time a number of Triassic-aged igneous rocks, including alkaline rocks and some magma mafic to felsic in composition, have occurred in the northern NCC (Zhang *et al.* 2012). Following this, massive intrusive rocks and widespread volcanic rocks of late Mesozoic age have been identified within the entire Eastern Block.

The eastern Hebei – western Liaoning area is located on the northern part of the NCC. Widespread intermediate-mafic dykes and several granitic intrusions, including the Baizhangzi (BZZ) granites, Dashizhuzi and Dushan complex, intruded into the Archean amphibolites and Mesoproterozoic littoral-neritic sediments (Fig. 1b, c). The exposed DSZZ complex is elliptical, approximately 20 × 7 km, and comprises granites and granodiorites as well as localized mafic enclaves including hornblende pyroxenites and diorites. Zircon U–Pb dating of the DSZZ granodiorites yields a weighted mean age of 224 Ma (Ye *et al.* 2014). The Dushan complex is located to the SW of the DSZZ complex, and was dated at 221–223 Ma (zircon U–Pb age; Luo *et al.* 2003; Ye *et al.* 2014). The BZZ granites, with a scale of approximately 600 × 200 m, crop out to the north of the DSZZ complex and were dated at 222 Ma (Luo *et al.* 2004). The large amount of exposed lamprophyre and granite dykes within the DSZZ complex and the BZZ granites range over 0.5–3 m in width and are hundreds of metres in length. Individual dykes mostly strike 28–58° NE and dip 37–67° towards the SE.

3. Samples

The granite samples of the DSZZ complex were collected for chemical and isotopic analyses. A composite (HGY-1) that consists of granite samples HGY-1, HGY-4 and HGY-5 was used for zircon U–Pb dating. Sampling locations are shown in Figure 1b. Some lamprophyre dyke samples were collected from underground, and the remainders were collected in the interior of the DSZZ complex (Fig. 1b–d). Both lamprophyre dyke samples in the interior of the DSZZ complex and the BZZ granites were collected for chemical and isotopic analyses. Two (SCYM-2 and SCYM-12) of them were chosen for zircon U–Pb dating.

The granites are coarse–medium grained with a mineral assemblage of K-feldspar (30–35 %) + quartz (20–30 %) + plagioclase (25–35 %) + hornblende ± biotite and typical granular texture. Sphene, zircon and magnetite are common accessory minerals. K-feldspar and plagioclase are partly altered to kaolinite.

All rock types of lamprophyres are mainly minette and kersantite with porphyritic texture. The phenocrysts are commonly biotite (or phlogopite, 30–40 %) ± minor plagioclase. These dykes contain various amounts of plagioclase, minor Fe–Ti oxide and quartz as groundmass phases. The biotite and phlogopite are partly altered to sericite and chlorite.

4. Analytical techniques

4.a. Zircon U–Pb isotope dating by LA-ICP-MS

Hand-picked zircon grains were mounted in epoxy blocks and polished until approximately two-thirds of grains were remained. U–Pb dating analyses were conducted by laser ablation inductively coupled plasma mass spectrometer (LA-ICP-MS; laser-ablation system GeoLas 2005 connected with an Agilent 7500a ICP-MS instrument) at the State Key Laboratory of Geological Processes and Mineral Resources (GPMR), China University of Geosciences, Wuhan. All data were acquired in single spot mode at a spot size of 32 μm. Detailed operating conditions for the laser-ablation system and the ICP-MS instrument were described by Liu *et al.* (2008, 2010*b*). Off-line data reduction was performed by ICPMS DataCal 9.0 (Liu *et al.* 2008). Concordia diagrams and weighted mean age calculations were made using IsoPlot 3.0 (Ludwig, 2003).

4.b. *In situ* Hf isotope analyses of zircon by LA-MC-ICP-MS

Hafnium isotopic analyses were conducted using a multi-collector ICP-MS (MC-ICP-MS, Neptune Plus) in combination with a laser ablation system (GeoLas

2005) at the GPMR. All data were acquired at a spot size of 44 μm. Detailed operating conditions can be found in Hu *et al.* (2012). Isobaric interference of ^{176}Yb on ^{176}Hf was corrected by measuring ^{173}Yb isotope and using $^{176}Yb/^{173}Yb = 0.7876$ (McCulloch, Rosman & De Laeter, 1977). The relatively minor interference of ^{176}Lu on ^{176}Hf was corrected by measuring the intensity of ^{175}Lu isotope and using the recommended $^{176}Lu/^{175}Lu = 0.02656$ (Blichert-Toft, Chauvel & Albarède, 1997). Off-line data reduction was performed by ICPMS DataCal 9.0 (Liu *et al.* 2010*a*).

4.c. Major- and trace-element measurements

Whole-rock samples were crushed and powdered in an agate ring mill to greater than 200 meshes. Major-element concentrations were determined by ME-XRF06 with analytical errors less than 3 % at the ALS Minerals in Guangzhou, China. Trace-element concentrations were measured by an inductively coupled plasma time-of-flight mass spectrometer (ICP-TOF-MS; OptiMass 9500) at the State Key Laboratory of Biogeology and Environmental Geology, China University of Geosciences, Wuhan. The samples were completely dissolved in Teflon bombs using a mixture of $HF + HNO_3$. Analyses of BCR-2 and GSR-3 indicate analytical accuracy is mostly better than 8 % in relative error.

4.d. Sr–Nd isotope analyses

Whole-rock powders were digested by bomb dissolution with a mixture of $HF + HNO_3$. Sr and Nd compositions were determined by a Finnigan MAT 261 thermal ionization mass spectrometer (TIMS) at the GPMR. Detailed analytical techniques are similar to those of Ling *et al.* (2009). Procedural blanks were about 2.0 ng and 0.12 ng for Sr and Nd, respectively. The measured values for the GBW04411 (K-feldspar) and La Jolla standards were $^{87}Sr/^{86}Sr = 0.75992 \pm 0.00010$ (2σ), $^{143}Nd/^{144}Nd = 0.511845 \pm 0.000012$ (2σ). $^{87}Sr/^{86}Sr$ ratios were normalized to $^{86}Sr/^{88}Sr = 0.1194$ and $^{143}Nd/^{144}Nd$ ratios were normalized to $^{146}Nd/^{144}Nd = 0.7219$. The $^{87}Rb/^{86}Sr$ and $^{147}Sm/^{144}Nd$ ratios were calculated using the Rb, Sr, Sm and Nd concentrations obtained by the ICP-TOF-MS.

5. Results

5.a. Zircon U–Pb geochronology

5.a.1. DSZZ granites

Results are shown in online Supplementary Table S1 (available at http://journals.cambridge.org/geo) and Figures 2 and 3a. Zircons from granite HGY-1 are light brown, transparent and euhedral to subhedral, with length/width ratios varying from 1 to 3 and lengths generally ranging from 70 to 180 μm. The cathodoluminescence (CL) images show that zircons contain typical magmatic oscillatory zoning. A total of 18 zircons were analysed at 19 points. With the exception of one point (HGY-1-12), the U–Pb data fall in a concentrated area and are all near-concordant in the concordant diagram. The core (HGY-1-6) is younger than the rim (HGY-1-5) in one grain, which may imply Pb loss. Two points yield an Early Triassic age ($^{206}Pb/^{238}U$ age) of 242 ± 6 Ma and 244 ± 6 Ma. The remaining 16 analyses yield a weighted mean $^{206}Pb/^{238}U$ age of 226 ± 3 Ma (2σ, MSWD = 3.6, $n = 16$).

5.a.2. Lamprophyre dykes

Zircons from dyke SCYM-2 are light green to transparent and rounded, irregular in external form, and of length ranging from 50 to 140 μm. The CL images show that some grains have both dark cores and bright rims, and some grains are structureless (Fig. 3b). A total of 10 zircons were analysed at 10 points; 9 of these are near-concordant to moderately concordant, and yield a weighted mean $^{207}Pb/^{206}Pb$ age of 2494 ± 23 Ma (2σ, MSWD = 0.23, $n = 9$). The remaining analysis (SCYM-2-3) yields a late Carboniferous age of 301 ± 6 Ma. Although the zircon grain is dark in the CL image, magmatic oscillatory zoning still occurs within the grain; this indicates that it was probably captured from igneous rocks of upper Palaeozoic age.

Lamprophyre dyke SCYM-12 has complex zircon populations (Fig. 3c, d), and 48 zircons were analysed at 48 points. Thirty-one of them demonstrate an Archean-Palaeoproterozoic age, and they can be divided into four groups with $^{207}Pb/^{206}Pb$ age ranges of 2660–2610 Ma, 2530–2440 Ma, 2330–2200 Ma and 1980–1830 Ma. All these grains are rounded in external form and have no obvious oscillatory zoning in CL images. A Mesoproterozoic age ($^{207}Pb/^{235}U$ ages of 1453–1254 Ma) was demonstrated by two near-concordant zircon grains, and two near-concordant zircon grains record a Neoproterozoic age ($^{206}Pb/^{238}U$ ages of 923–805 Ma). Except for two less-concordant points, six zircon grains have significant oscillatory zoning and show widely scattered near-concordant $^{206}Pb/^{238}U$ ages of Middle Ordovician – Middle Triassic. The remaining four zircon grains, with significant oscillatory zoning, yield a weighted mean $^{206}Pb/^{238}U$ age of 167 ± 8 Ma (2σ, MSWD = 4.4, $n = 4$).

5.b. Major and trace elements

5.b.1. DSZZ granites

The major- and trace-element data are reported in Table 1. The DSZZ granites have SiO_2 contents ranging from 65.9 to 70.8 wt %. All samples are relatively high in Al_2O_3 (14.7–15.1 wt %), Na_2O (4.5–4.9 wt %) and total alkalis ($K_2O + Na_2O$ ranging over 8.5–9.2 wt %), with Na_2O/K_2O ratios of 0.96–1.25. By contrast, they are low in P_2O_5 (0.10–0.24 wt %) and

https://doi.org/10.1017/S0016756817000437 Published online by Cambridge University Press

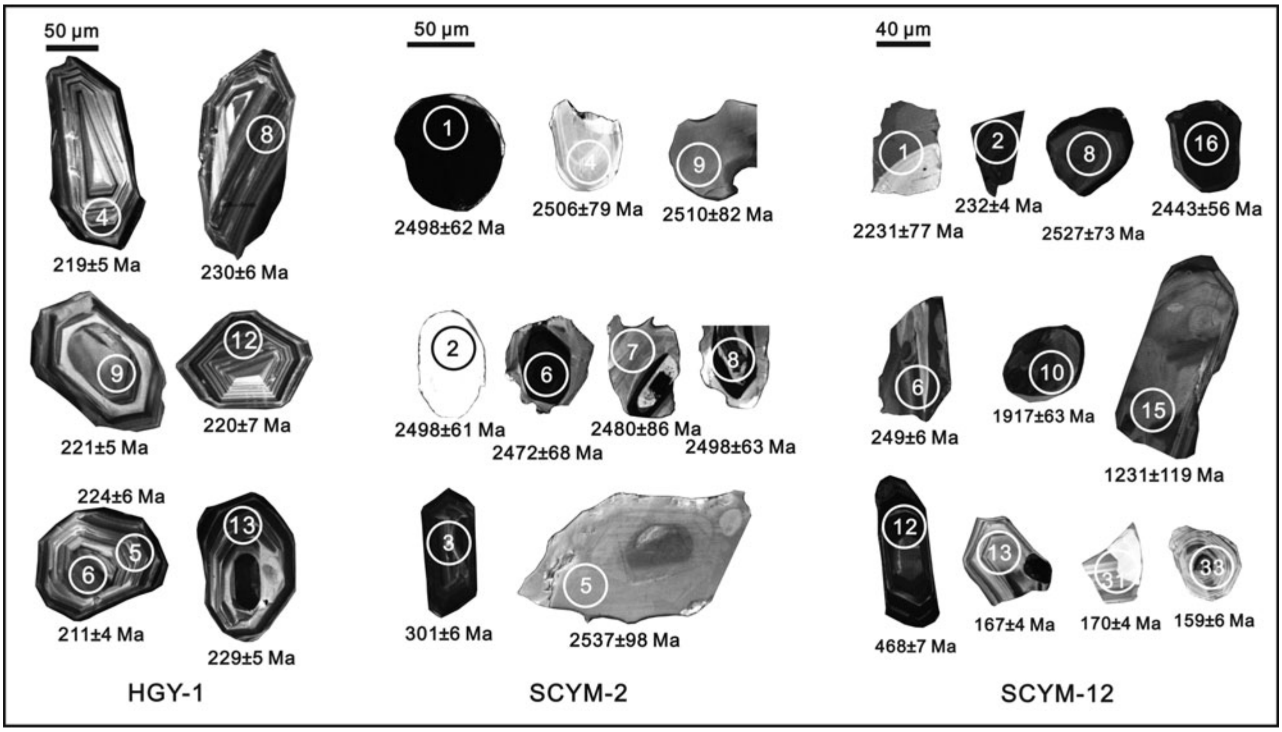

Figure 2. Cathodoluminescence images of zircons. White and black circles are LA-ICP-MS analysis spots.

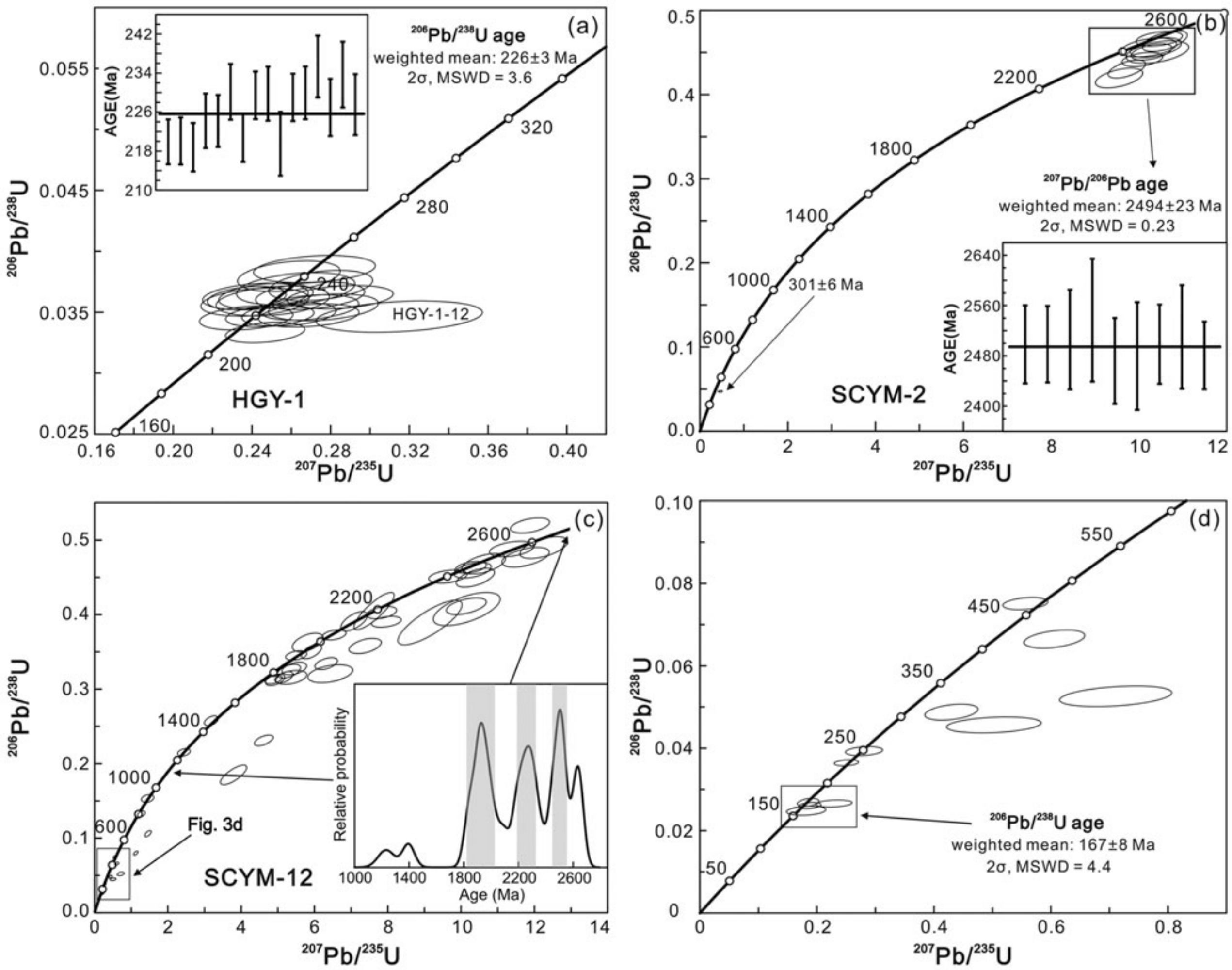

Figure 3. Zircon U–Pb age of (a) the Dashizhuzi granites (HGY-1) and (b–d) lamprophyre dykes (SCYM-2 and SCYM-12).

https://doi.org/10.1017/S0016756817000437 Published online by Cambridge University Press

Table 1. Major- and trace-element concentrations of the Dashizhuzi granites and the lamprophyre dykes

	DSZZ granites						Group 2 dykes		Group 1 dykes				
Sample	HGY-1	HGY-2	HGY-3	HGY-4	HGY-5	HGY-6	SCYM-2	SCYM-15	SCYM-5	SCYM-11	SCYM-12	SCYM-16	SCYM-17
Major elements (wt %)													
SiO_2	70.77	65.90	69.38	69.59	69.28	69.03	49.09	51.96	55.29	56.42	54.58	48.49	53.73
Al_2O_3	14.91	15.08	15.02	14.74	14.87	15.01	11.70	12.43	14.10	14.03	13.42	12.37	14.14
Fe_2O_3	1.69	3.58	2.09	2.16	2.09	1.83	7.95	7.37	5.29	6.65	6.43	7.95	6.80
CaO	0.85	2.59	1.44	1.66	1.48	1.58	5.88	5.19	5.88	2.71	5.06	8.16	6.14
MgO	0.52	1.86	0.67	0.80	0.81	0.46	13.69	11.72	6.34	7.90	7.16	9.67	5.70
Na_2O	4.64	4.69	4.87	4.59	4.58	4.48	1.30	2.63	3.65	3.12	3.25	2.50	3.85
K_2O	4.54	3.76	4.33	4.23	4.59	4.68	4.98	2.58	3.55	4.38	4.99	4.21	4.59
TiO_2	0.27	0.44	0.34	0.32	0.31	0.35	1.05	0.73	0.84	0.81	0.80	1.23	0.99
P_2O_5	0.10	0.24	0.13	0.13	0.12	0.14	0.63	0.46	0.94	0.77	0.78	0.99	0.83
LOI	0.68	1.16	1.10	0.64	0.68	1.64	2.42	3.66	3.42	2.05	2.01	3.06	2.42
Total	99.19	99.68	99.61	99.12	99.07	99.41	99.31	99.25	99.68	99.36	99.18	99.11	99.79
Mg no.	37.9	50.7	38.8	42.3	43.4	33.2	77.3	75.9	70.3	70.2	68.8	70.7	62.4
Trace elements (ppm)													
Li	16.2	27.4	26.6	12.9	20.9	14.2	38.7	30.7	16.3	26.4	24.7	42.7	26.5
Be	2.55	1.77	2.29	2.33	2.97	3.77	2.27	2.41	2.70	3.71	3.60	3.89	3.33
Sc	2.57	5.89	3.55	3.13	3.40	3.33	17.40	18.30	14.35	13.60	14.80	21.00	16.40
Ti	2047	2511	2200	1871	1965	2269	6039	4510	4715	4435	4612	6858	5909
V	18.9	59.1	29.6	27.9	28.2	34.7	139.0	142.0	134.0	119.0	125.0	165.0	147.0
Cr	124.0	103.0	129.0	119.0	116.0	122.0	712.0	563.0	218.0	275.0	290.0	461.0	174.0
Mn	304	351	232	292	308	244	882	734	457	416	672	796	718
Ni	7.8	9.2	12.9	10.6	11.5	11.7	45.4	69.1	45.1	21.6	24.8	30.9	23.2
Co	53.3	30.4	67.2	46.3	56.1	94.9	470.0	360.0	170.5	94.5	102.0	116.0	50.7
Cu	1.8	5.9	3.5	2.1	2.2	3.5	149.0	27.9	21.7	14.4	57.1	65.2	63.5
Zn	28.9	36.9	34.7	28.6	28.2	33.2	103.0	64.0	61.1	89.4	71.9	90.0	68.2
Ga	34.9	41.7	35.8	36.7	39.4	37.1	51.5	45.9	41.7	65.4	84.0	37.6	72.9
Rb	101.0	68.9	73.0	87.5	92.5	122.0	161.0	68.2	74.8	78.7	97.8	119.0	98.6
Sr	463	1042	696	668	679	458	1011	1004	849	1003	1673	943	1618
Y	5.7	8.3	7.8	7.3	7.6	7.0	14.2	11.7	27.0	17.9	18.0	24.6	18.6
Zr	151	217	188	148	154	211	158	167	268	329	321	461	357
Nb	17.7	16.4	21.3	17.4	18.8	20.6	8.3	9.1	7.9	16.4	15.5	9.5	16.6
Cd	1.25	2.81	1.88	0.98	1.61	4.11	13.90	5.15	4.51	3.07	2.86	5.04	3.34
Ba	1281	1711	1298	1356	1480	1357	2293	1989	1632	2434	3289	1557	2840
La	37.4	46.4	42.4	37.9	36.0	46.9	56.3	40.7	201.5	101.0	102.0	79.0	95.1
Ce	58.9	76.9	68.1	60.9	63.4	68.4	159.0	80.3	459.0	346.0	340.0	308.0	339.0
Pr	5.7	8.2	7.0	6.0	6.4	6.8	13.3	9.7	30.5	20.7	21.2	22.0	21.9
Nd	18.4	27.6	23.4	20.4	19.9	21.3	35.9	38.4	128.0	75.6	77.3	89.1	83.9
Sm	2.85	4.37	3.73	3.19	3.39	3.26	9.73	6.91	24.25	13.50	14.20	18.00	14.30
Eu	0.87	1.36	1.19	1.07	1.05	1.08	2.58	1.97	5.83	3.72	4.06	4.68	3.81
Gd	2.25	3.45	2.97	2.49	2.66	2.71	6.98	4.75	16.80	9.65	9.40	12.90	9.91
Tb	0.24	0.37	0.32	0.29	0.30	0.28	0.82	0.53	1.83	1.04	1.05	1.43	1.06
Dy	1.15	1.73	1.57	1.34	1.34	1.26	3.21	2.37	6.54	3.99	3.98	5.93	4.19
Ho	0.19	0.27	0.26	0.23	0.24	0.23	0.52	0.42	0.95	0.64	0.62	0.87	0.66
Er	0.60	0.83	0.76	0.73	0.72	0.74	1.48	1.21	2.54	1.77	1.79	2.26	1.86
Tm	0.08	0.12	0.12	0.11	0.11	0.12	0.18	0.16	0.28	0.23	0.22	0.26	0.22
Yb	0.58	0.73	0.75	0.74	0.73	0.70	1.02	0.98	1.58	1.36	1.27	1.59	1.41
Lu	0.10	0.13	0.13	0.11	0.12	0.14	0.16	0.15	0.25	0.22	0.21	0.25	0.21
Hf	nd[a]	4.84	nd	nd	nd	nd	3.99	4.42	6.42	8.14	7.80	11.30	8.60
Ta	1.90	1.27	2.80	2.44	2.82	3.29	1.25	1.46	1.36	2.13	1.97	1.46	1.96
Pb	27.2	25.2	27.4	25.4	24.8	26.1	21.4	9.5	21.2	29.5	25.8	11.3	19.2
Th	14.1	11.9	14.1	13.5	12.6	15.0	9.7	5.5	30.6	20.3	20.2	13.8	15.8
U	1.87	2.34	1.87	2.77	2.19	2.97	1.65	1.53	4.61	6.13	5.61	3.65	4.17
REE	129.29	172.42	152.74	135.54	136.35	153.95	291.18	188.53	879.78	579.42	577.30	546.27	577.53
δEu	1.01	1.03	1.06	1.12	1.03	1.08	0.91	0.99	0.84	0.95	1.01	0.89	0.93
$(La/Yb)^N$	46.3	45.6	40.6	36.7	35.4	48.1	39.6	29.8	91.8	53.3	57.6	35.6	48.4
$(Gd/Yb)^N$	3.2	3.9	3.3	2.8	3.0	3.2	5.7	4.0	8.8	5.9	6.1	6.7	5.8
Dy/Yb	1.98	2.37	2.09	1.81	1.84	1.80	3.15	2.42	4.14	2.93	3.13	3.73	2.97
Sr/Nd	25.2	37.8	29.7	32.7	34.1	21.5	28.2	26.1	6.6	13.3	21.6	10.6	19.3
Sr/Y	81.7	126.3	89.2	91.4	89.2	65.3	71.2	85.8	31.5	56.0	92.9	38.3	87.0
Th/U	7.5	5.1	7.5	4.9	5.8	5.1	5.9	3.6	6.6	3.3	3.6	3.8	3.8
Ba/Sr	2.8	1.6	1.9	2.0	2.2	3.0	2.3	2.0	1.9	2.4	2.0	1.7	1.8
Ba/Th	90.9	143.8	92.1	100.4	117.5	90.5	236.9	364.3	53.4	119.9	162.8	112.8	179.7
Ce/Pb	2.2	3.1	2.5	2.4	2.6	2.6	7.4	8.5	21.7	11.7	13.2	27.3	17.7
Rb/Sr	0.22	0.07	0.10	0.13	0.14	0.27	0.16	0.07	0.09	0.08	0.06	0.13	0.06
Ba/Rb	12.7	24.8	17.8	15.5	16.0	11.1	14.2	29.2	21.8	30.9	33.6	13.1	28.8
K/Yb[b]	65.0	42.8	47.9	47.5	52.2	55.5	39.3	20.6	17.7	26.1	31.8	20.9	26.2

[a]nd: data not detected; [b]K/Yb = weight (K/Yb)/1000

https://doi.org/10.1017/S0016756817000437 Published online by Cambridge University Press

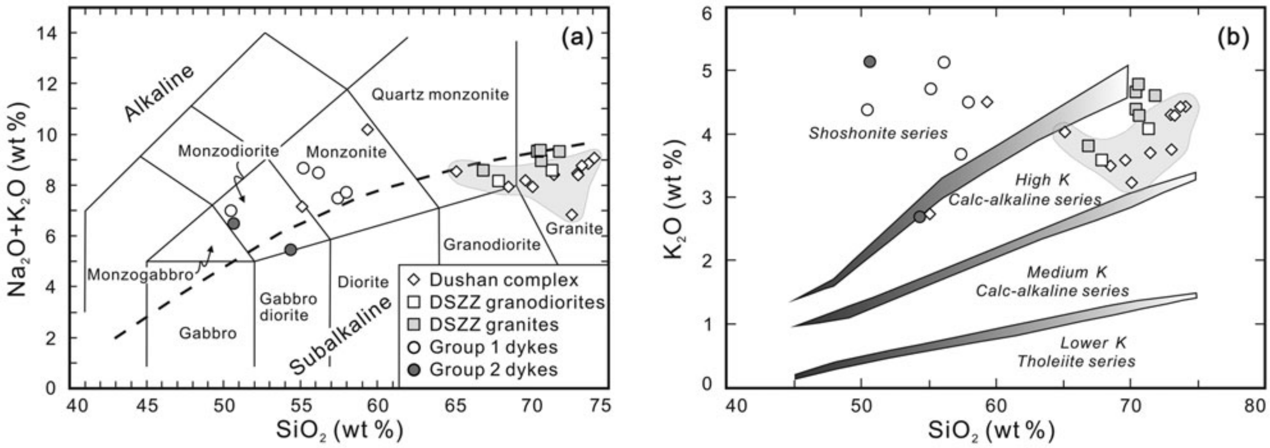

Figure 4. (a) SiO_2 v. Na_2O+K_2O and (b) SiO_2 v. K_2O for the Dashizhuzi granites and lamprophyre dykes. The data for Dushan complex and Dashizhuzi granodiorites are from Ye *et al*. (2014).

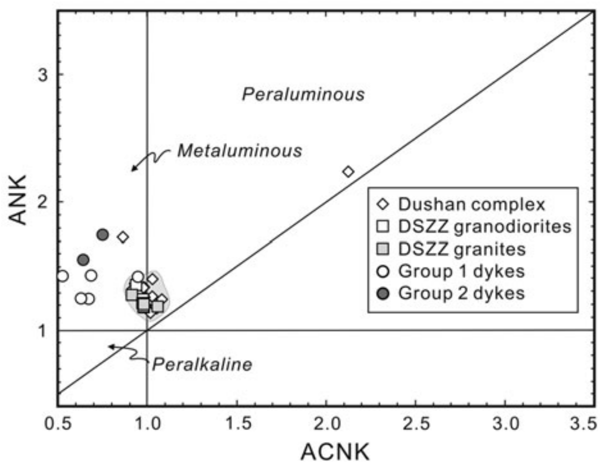

Figure 5. Plot of A/CNK v. ANK for the Dashizhuzi granites and lamprophyre dykes. The data for Dushan complex and Dashizhuzi granodiorites are from Ye *et al*. (2014).

TiO_2 (0.27–0.44 wt %) abundances, and have Mg no. of 33–51 (Mg no. = 100 × molar Mg/(Mg + Fe)). The DSZZ granites have SiO_2 contents comparable to those of the DSZZ granodiorites and the Dushan complex (Ye *et al*. 2014), but with relatively higher total alkali contents. In the total alkali versus silica diagram (Fig. 4a), all samples plot in granite and quartz monzonite fields. These granite rocks are metaluminous (Fig. 5) and can be categorized to high-K calc-alkaline series rocks (Fig. 4b).

The DSZZ granites have total rare Earth element contents (ΣREE) varying over 129–172 ppm, and display right-dipping chondrite-normalized REE patterns (Fig. 6b) with $(La/Yb)_N$ and $(Gd/Yb)_N$ ratios of 35–48 and 2.8–3.9, respectively. All samples are distinctive for their extremely low heavy REE (HREE) abundances when compared to typical ocean island basalt (OIB; Sun & McDonough, 1989) and LCC of the NCC (Gao *et al*. 1998). The patterns have slightly positive Eu anomalies (1.01–1.12; $\delta Eu = (Eu)_N/(0.5\times[(Sm)_N+(Gd)_N])$, where the subscript N denotes chondrite-normalized value). The primitive mantle-normalized trace-element patterns are similar to those of the DSZZ granodiorites (Ye *et al*. 2014) and LCC of the NCC (Fig. 6a). All samples are enriched by large-ion lithophile elements (LILE; e.g. K, Rb, Sr, Ba, U) and depleted in high-field-strength elements (HFSE; e.g. Nb, Ta, Ti, P), and display a strong positive Pb anomaly and moderate to strong negative Nb, Ta, Ti and P anomalies. They also have some other striking geochemical features, including high Sr/Y (65–126) and elevated Cr (103.0–129.0 ppm) abundances.

5.b.2. *Lamprophyre dykes*

The lamprophyre dykes display a wide range of SiO_2 abundances (48.5–56.4 wt %). They are all characterized by moderate to low Na_2O (1.3–3.9 wt %) and high abundances of total alkalis ($K_2O + Na_2O$ = 5.2–8.4 wt %). Two groups of dykes can be recognized based on their elemental features, especially MgO and Al_2O_3 contents. The Group 2 dykes include SCYM-2 and SCYM-15, and the remainder of the dykes belong to Group 1. The Group 1 dykes have moderate to high Al_2O_3 (12.4–14.1 wt %) contents and relatively low total Fe_2O_3 ($Fe_2O_3^T$, 5.3–8.0 wt %) and MgO (5.7–9.7 wt %) contents, with Mg no. of 62–71; the Group 2 dykes have relatively low Al_2O_3 (11.7–12.4 wt %) contents and relatively high $Fe_2O_3^T$ (7.4–8.0 wt %) and MgO (11.7–13.7 wt %) contents, with Mg no. of 76–77. All samples plot in the fields of monzodiorite and monzonite, and belong to shoshonite series rocks (Fig. 4a, b).

The Group 1 dykes are characterized by low Ni (21.6–45.1 ppm) and Sc (13.6–21.0 ppm) and moderate Co (51–171 ppm) and Cr (174–461 ppm) abundances, and significantly high ΣREE abundances (546–880 ppm). In contrast, the Group 2 dykes contain moderate Ni (45.4–69.1 ppm) and very high Co (360–470 ppm) and Cr (563–712 ppm) abundances, and low Sc (17.4–18.3 ppm) and ΣREE abundances (189–291 ppm). All these samples exhibit a wide range of ΣREE abundances, and display similar right-dipping chondrite-normalized REE patterns (Fig. 6d)

https://doi.org/10.1017/S0016756817000437 Published online by Cambridge University Press

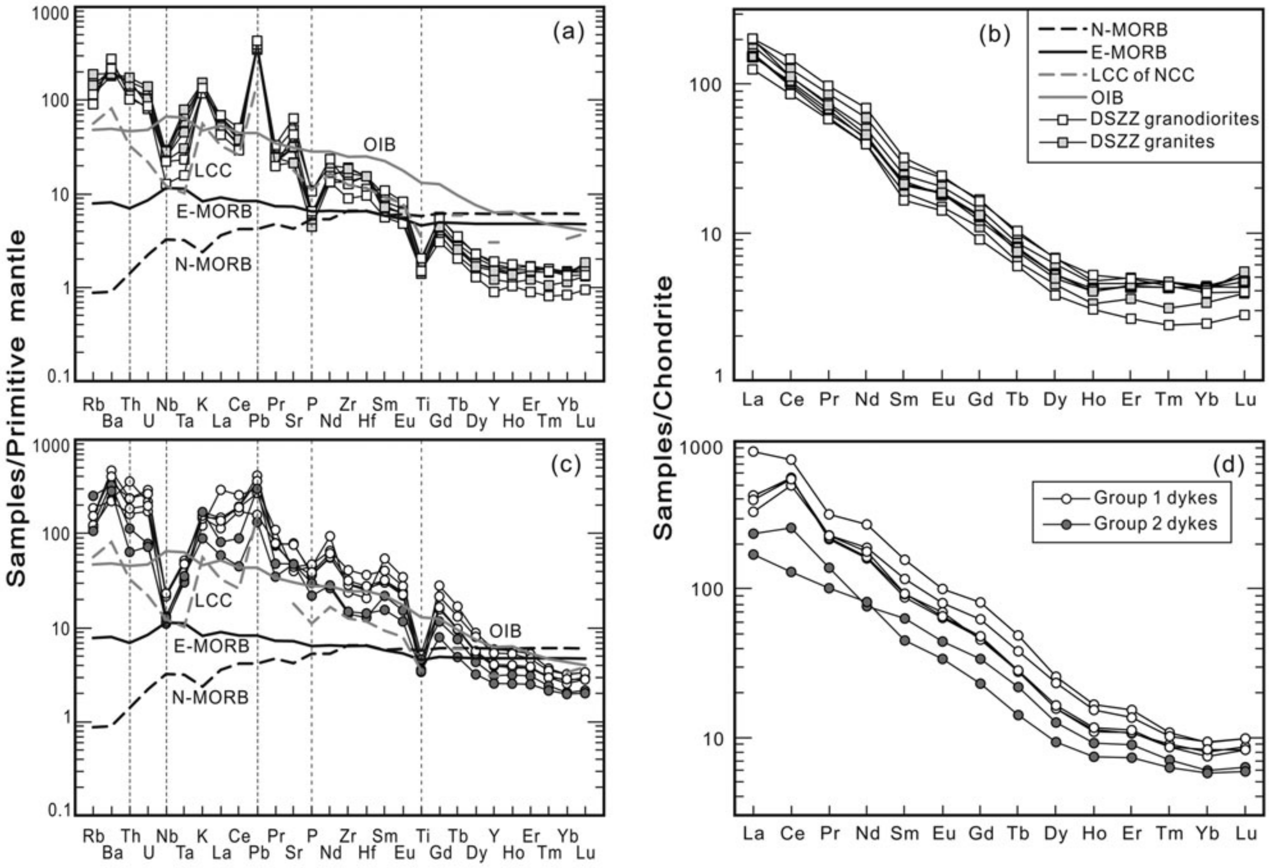

Figure 6. (a, c) Trace-element and (b, d) rare Earth element concentrations of the Dashizhuzi granites and lamprophyre dykes. Concentrations were normalized to primitive mantle and chondrite that were recommended by Sun & McDonough (1989). Data for OIB, N-MORB and E-MORB (Sun & McDonough, 1989) and LCC of the NNC (Gao *et al.* 1998) are presented for comparison. The data for the Dashizhuzi granodiorites are from Ye *et al.* (2014).

with $(La/Yb)_N$ and $(Gd/Yb)_N$ ratios of 30–92 and 4.0–8.8, respectively. The patterns have slightly negative Eu anomalies with δEu ranging from 0.84 to 1.01. All these lamprophyre dykes show subparallel primitive-normalized trace-element patterns (Fig. 6c). They are enriched in LILE (e.g. K, Rb, Sr, Ba, U), depleted in HFSE (e.g. Nb, Ta, Ti, P) and display a strong positive Pb anomaly, moderate to strong negative Nb, Ta and Ti anomalies and slightly negative P, Zr and Hf anomalies. The primitive mantle-normalized trace-element patterns are similar to those of LCC of the NCC to some extent, and abundances of most trace elements of the Group 2 dykes are comparable with those of OIB. The Group 1 dykes have Th/U (3.3–3.8, except SCYM-5), Ba/Th (53–180) and Ce/Pb (11.7–27.3) ratios similar to those of MORB (Salters & Stracke, 2004), whereas the Group 2 dykes have relatively higher Ba/Th (237–364) and lower Ce/Pb (7.4–8.5) ratios.

5.c. Whole-rock Sr–Nd isotopes

5.c.1. DSZZ granites

Sr and Nd isotope compositions are listed in Table 2. The DSZZ granites have Sr–Nd isotopic compositions plotting in the field of the Mesozoic lower crustal granulite xenoliths (Fig. 7a; Liu *et al.* 2004; She *et al.* 2006) and cumulates (Shao *et al.* 2006). The initial $^{87}Sr/^{86}Sr$ ratios (0.70416–0.70449) of the DSZZ granites are almost identical to those of coeval Hekanzi pyroxene-biotite syenite (Yang *et al.* 2012) and the Devonian Hongshila pyroxenite-hornblendite complex (Zhang *et al.* 2009*a*). They display a narrow range in Nd isotopes (ε_{Nd} (226 Ma) of –11.0 to –9.1), and have Nd model (TDM_{Nd}) ages of 1.42–1.58 Ga.

5.c.2. Lamprophyre dykes

The Group 1 dykes have initial $^{87}Sr/^{86}Sr$ ratios of 0.70569 to 0.70629 and have ε_{Nd} (167 Ma) values varying from –8.5 to –0.1. With the exception of SCYM-11, their Sr–Nd isotopic compositions overlap those of the Xinglonggou lavas (Gao *et al.* 2004). TDM_{Nd} ages of the Group 1 dykes range over 0.93–1.51 Ga. The Group 2 dykes have initial $^{87}Sr/^{86}Sr$ ratios of 0.70618–0.70800 and ε_{Nd} (167 Ma) values of –10.7 to –7.4. The significantly high $^{87}Sr/^{86}Sr$ ratio of SCYM-2 is possibly due to hydrothermal alterations, which is also supported by relatively high Rb, Cu and Zn contents. Their Sr–Nd isotopic compositions plot in the field of the Mesozoic alkaline rocks (Fig. 7b). TDM_{Nd} ages of the Group 2 dykes range over

https://doi.org/10.1017/S0016756817000437 Published online by Cambridge University Press

Table 2. Sr and Nd isotopic compositions of the Dashizhuzi granites and the lamprophyre dykes

Sample	Sm (ppm)	Nd (ppm)	$^{147}Sm^{a}/^{144}Nd$	$^{143}Nd/^{144}Nd$	2σ	$\varepsilon_{Nd}(t)^{b}$ (167 Ma)	$\varepsilon_{Nd}(t)^{b}$ (226 Ma)	$TDM_{Nd}{}^{c}$ (Ma)	$f_{Sm/Nd}$ $f_{Sm/Nd}$	Rb (ppm)	Sr (ppm)	$^{87}Rb/^{86}Sr$	$^{87}Sr/^{86}Sr$	2σ	$^{87}Sr/^{86}Sr(t)$ (167 Ma)	$^{87}Sr/^{86}Sr(t)$ (226 Ma)
DSZZ granites																
HGY-1	2.85	18.4	0.097	0.512001	2	−10.2	−9.5	1459	−0.52	101	463	0.631	0.706364	4	0.704866	0.704336
HGY-2	4.37	27.6	0.096	0.511923	3	−11.8	−11.0	1584	−0.51	69	1042	0.191	0.705061	6	0.704607	0.704446
HGY-3	3.73	23.4	0.096	0.512021	2	−9.9	−9.2	1467	−0.51	73	696	0.303	0.705463	5	0.704743	0.704488
HGY-5	3.39	19.9	0.103	0.512027	3	−9.9	−9.2	1546	−0.48	93	679	0.394	0.705729	6	0.704793	0.704462
HGY-6	3.26	21.3	0.093	0.512020	3	−9.8	−9.1	1422	−0.53	122	458	0.771	0.706639	7	0.704809	0.704162
Lamprophyre dykes: Group 2																
SCYM-2	9.73	35.9	0.164	0.512225	4	−7.4	−7.1	2819	−0.17	161	1011	0.461	0.709096	4	0.708002	0.707615
SCYM-15	6.91	38.4	0.109	0.511995	3	−10.7	−10.0	1677	−0.45	68	1004	0.197	0.706643	6	0.706176	0.706011
Lamprophyre dykes: Group 1																
SCYM-5	23.50	126.0	0.113	0.512539	3	−0.1	0.5	925	−0.43	72	822	0.253	0.706888	6	0.706288	0.706076
SCYM-11	13.50	75.6	0.108	0.512105	2	−8.5	−7.8	1506	−0.45	79	1003	0.227	0.706735	6	0.706196	0.706005
SCYM-16	18.00	89.1	0.122	0.512537	3	−0.4	0.2	1023	−0.38	119	943	0.365	0.706558	5	0.705691	0.705385

[a] ^{147}Sm decay constant is 6.54×10^{-12} a^{-1}; [b] ε_{Nd} (t) is calculated with $^{143}Nd/^{144}Nd = 0.512638$ and $^{147}Sm/^{144}Nd = 0.1966$ for present-day CHUR (Hamilton *et al.* 1983); [c] Nd model age (TDM_{Nd}) is calculated with $^{143}Nd/^{144}Nd = 0.51315$ and $^{147}Sm/^{144}Nd = 0.2135$ for present-day depleted mantle (Goldstein, O'Nions & Hamilton, 1984; Peucat *et al.* 1989)

1.68–2.82 Ga, which is significantly older than the Group 1 dykes.

5.d. Zircon Hf isotopes

5.d.1. DSZZ granites

Results for *in situ* Hf isotope analyses of zircons are shown in online Supplementary Table S2 (available at http://journals.cambridge.org/geo) and Figure 8. Zircons from the DSZZ granites have model ages (TDM_{Hf}) of 0.95–1.36 Ga and a wide range of $\varepsilon_{Hf}(t)$ values varying from –12.2 to –1.4 with a trend towards the CHUR line recommended by Bouvier, Vervoort & Patchett (2008).

5.d.2. Lamprophyre dykes

The ancient zircons of the lamprophyre dyke SCYM-2 have TDM_{Hf} ages of 2.67 Ga and $\varepsilon_{Hf}(t)$ values varying over 3.2–4.5, which lie close to the depleted mantle and mafic-granulite-xenoliths-hosted ancient zircons evolution line (Zheng *et al.* 2004*a*) at this time beneath the NCC (Fig. 8).

6. Discussion

6.a. Emplacement age

Previous studies have shown that zircons are used to track complicated thermal histories. Similarly, most tectono-thermal histories of the NCC are recorded by zircon U–Pb geochronology of the DSZZ granites and the lamprophyre dykes. Four Precambrian age groups of 2.66–2.61 Ga, 2.53–2.44 Ga, 2.33–2.20 Ga and 1.98–1.83 Ga are recognized from zircons within the lamprophyre dykes SCYM-2 and SCYM-12 (online Supplementary Table S1, available at http://journals.cambridge.org/geo, and Fig. 3b, c). The Archean age group of 2.66–2.61 Ga is identical to their *in situ* hafnium model ages (2.67 Ga). These zircons also have high ε_{Hf} (2.67 Ga) values from +3.2 to +4.5, which probably reflects a depleted-mantle-derived Precambrian continental crust growth event. The age group of 2.53–2.44 Ga coincides with a widespread metamorphism and deformation event during late Archean time (*c.* 2.5 Ga) in the NCC (e.g. Pidgeon, 1980; Jahn & Zhang, 1984; Jin, Li & Liu, 1991; Wu *et al.* 1991; Kröner *et al.* 1998). The Palaeoproterozoic age group of 2.33–2.20 Ga is roughly coeval with the development and closure of the Jiao-Liao-Ji continental rift in the Palaeoproterozoic (2.2–1.9 Ga; e.g. Li *et al.* 2005; Zhao *et al.* 2005), and the younger age group of 1.98–1.83 Ga probably marks the final collision of the Western and Eastern blocks of the NCC during late Palaeoproterozoic time (*c.* 1.85 Ga; Zhao *et al.* 2001, 2005). Further, two Palaeozoic age groups of 468–416 Ma and 331–289 Ma obtained from the lamprophyre dykes, SCYM-2 and SCYM-12, coincide well with the complicated evolution histories of the Palaeo-Asian Ocean (e.g. Windley *et al.* 2007)

https://doi.org/10.1017/S0016756817000437 Published online by Cambridge University Press

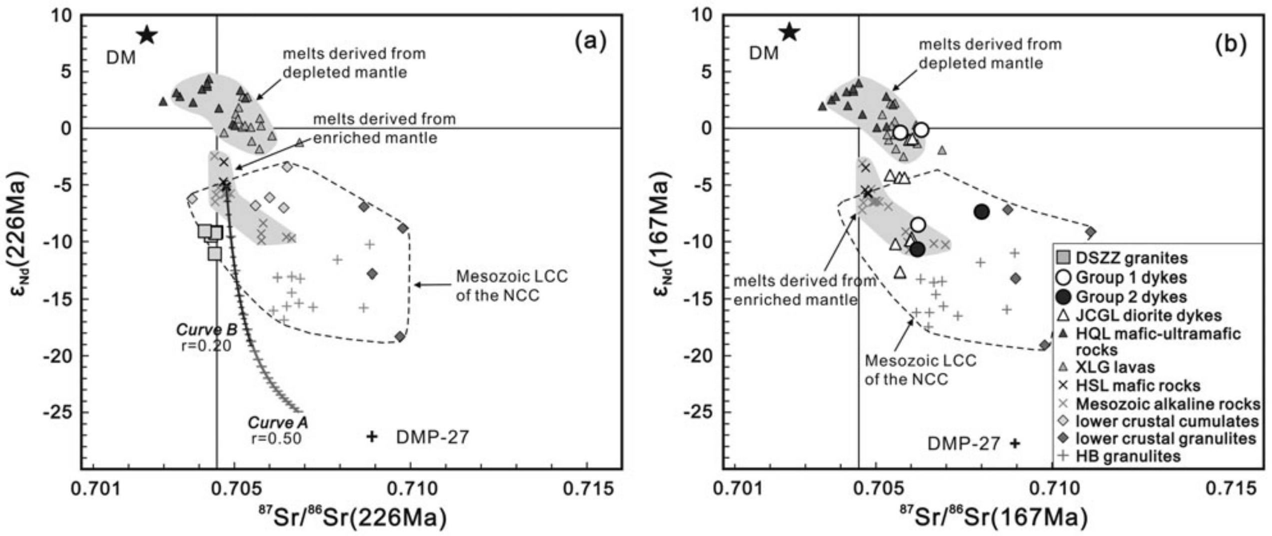

Figure 7. Nd and Sr isotopic compositions of (a) the Dashizhuzi granites and (b) lamprophyre dykes. The black and grey curves A and B in (a) with horizontal tick marks are AFC (assimilation and fractional crystallization) trends showing 5 % increments in F (magma remaining) for melts of enriched mantle (Hongshila pyroxenite; Zhang *et al*. 2009*a*) that assimilate lower crust (DMP-27; Liu *et al*. 2004). Fields for melts derived from depleted mantle are the Triassic Hongqiling-Piaohechuan (HQL) mafic-ultramafic rocks (Wu *et al*. 2004) and the Jurassic Xinglonggou (XLG) lavas (Gao *et al*. 2004); for melts derived from enriched mantle the Triassic alkaline magma rocks (Yang *et al*. 2012; Zhang *et al*. 2012) and the Devonian Hongshila (HSL) pyroxenite-hornblendite complex (Zhang *et al*. 2009*a*); and for Mesozoic LCC of the NCC the Hannuoba (HB) deep-seated mafic-intermediate xenoliths (Liu *et al*. 2004) and early Mesozoic lower crustal cumulates (Shao *et al*. 2006) and granulites (Shao *et al*. 2006; She *et al*. 2006). Data for Jingchanggouliang (JCGL) diorite dykes (Fu *et al*. 2012*a*) are present for comparison. All data are calculated at 226 Ma in (a) and 167 Ma in (b).

and the Carboniferous–Permian (330–265 Ma) collision of the NCC and the Mongolia composite terranes (e.g. Windley *et al*. 2007; Zhang *et al*. 2010*a*). Another considerable Phanerozoic period (249–240 Ma) is also recorded by zircons from the granite HGY-1 and lamprophyre dykes SCYM-12, and may be related to post-collisional extension or the granulite metamorphism induced by basaltic underplating (Shao, Han & Li, 2000).

The youngest group from the granite HGY-1 yields a weighted mean ^{206}Pb/^{238}U age of 226 ± 3 Ma (Fig. 3a), which is consistent with the reported zircon U–Pb age (224 ± 2 Ma) of the DSZZ granodiorites by Ye *et al*. (2014). This age probably represents the best estimate of the crystallization age of the DSZZ granites. The DSZZ complex therefore emplaced during Middle Triassic time. This period is also implied by many exposed Triassic alkaline, mafic-ultramafic and felsic magma rocks along the northern margin of the NCC (online Supplementary Table S3 and Supplementary Figure S1; e.g. Yan *et al*. 2000; Luo *et al*. 2003; Wu, Yang & Liu, 2005; Pei *et al*. 2008; Fu *et al*. 2012*a*; Ye *et al*. 2014).

Zircon grains from the lamprophyre dykes SCYM-2 and SCYM-12 are mainly inherited from early igneous and metamorphic rocks. The Middle Jurassic age of 167 ± 8 Ma is recorded by four zircon grains that are euhedral to subhedral in external form (Figs 2, 3d). This is consistent with the field relationships demonstrating that these dykes are hosted in the interior of the Middle Triassic DSZZ complex. Furthermore, the

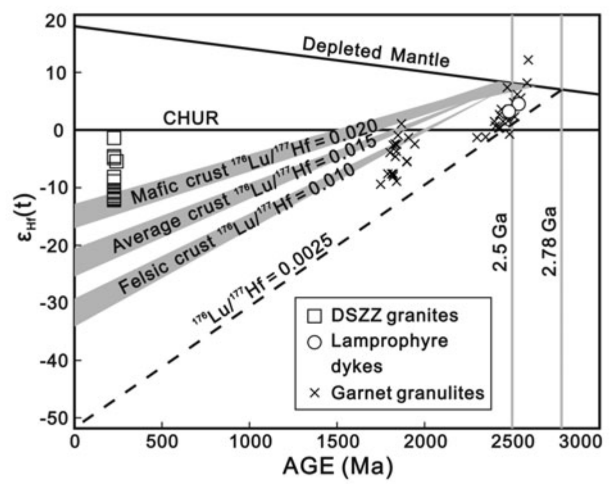

Figure 8. Plots of $\varepsilon_{Hf}(t)$ against U–Pb age for the Dashizhuzi granites and lamprophyre dykes. The dashed line with (^{176}Lu/^{177}Hf = 0.0025), representing trend of zircons in the Fuxian garnet granulite xenoliths (Zheng *et al*. 2004*a*), is shown for comparison. The mafic crust, felsic crust and average crust evolution line with assumed ^{176}Lu/^{177}Hf ratios of 0.020, 0.010 and 0.015, respectively, are presented for comparison.

occurrence of voluminous intermediate to felsic granitoids and volcanic rocks in the NE segment of the NCC (e.g. Miao *et al*. 1998; Gao *et al*. 2004; Wu *et al*. 2006*a*; Du *et al*. 2007) suggests a Middle–Late Jurassic pronounced magmatism period. The Middle Jurassic age of 167 ± 8 Ma is therefore the best estimate for emplacement age of these lamprophyre dykes.

Table 3. Elemental ratios and isotopic data used for the AFC modelling for curves A and B (EM – enriched lithospheric mantle; LCC – lower continental crust)

	$^{87}Sr/^{86}Sr(t)$ 226 Ma	$\varepsilon_{Nd}(t)$ 226 Ma	Sr/Nd	References
EM	0.704771	– 5.1	15.7	Zhang *et al.* (2009*a*) ; Yang *et al.* (2012)
LCC	0.708910	– 27.1	2.0	Liu *et al.* (2004)

6.b. Source of the DSZZ granites

The distinctive features of high Na_2O (≥4.4 wt %) and Sr (≥458 ppm), enrichment in LREE and extreme depletion in HREE, Nb–Ta and Y (≤ 8.3 ppm), with high Sr/Y (65–126) and $(La/Yb)_N$ ratios (35–48) of the DSZZ granites, are similar to those of adakitic magmas from island arcs and Archean TTG suites (Kay, 1978; Martin, 1999). As recognition of magma rocks with analogous characters has increased, several petrogenetic hypotheses have been proposed including: melts from subducted young oceanic crust followed by interaction with the overlying mantle wedge peridotite (e.g. Kay, 1978; Drummond & Defant, 1990; Schiano *et al.* 1995), melting of thickened mafic LCC (e.g. Atherton & Petford, 1993) or melting of foundered LCC (e.g. Xu *et al.* 2002, 2006*a*; Gao *et al.* 2004); melting of hydrated mantle peridotite (Stern & Hanson, 1991; MacPherson, Dreher & Thirlwall, 2006) or AFC (assimilation and fractional crystallization and/or crustal contamination) processes in basaltic magmas (e.g. Richards & Kerrich, 2007; Fu *et al.* 2012*b*); mixing of mafic and felsic magmas (Guo *et al.* 2007; Streck, Leeman & Chesley, 2007); and source inheritance (Ma *et al.* 2012, 2015). In the following discussion, we test these potential petrogenetic hypotheses in order to explain the petrologic and geochemical characteristics of the DSZZ granites.

Slab-melt–peridotite interaction has been proposed to account for the origin of rocks with adakitic characters (e.g. Kay, 1978; Schiano *et al.* 1995). This petrogenetic model requires a subduction setting in the northern margin of the NCC, yet the initial subduction of the Palaeo-Pacific Plate beneath the Eurasian continent took place during Early–Middle Jurassic time (Xu *et al.* 2013) and the original calc-alkaline volcanic rocks related to the subduction of Mongol-Okhotsk Ocean Plate occurred during Early Jurassic time in the Erguna Massif (Wu *et al.* 2011; Xu *et al.* 2013). These subduction events took place later than the emplacement of the DSZZ granites (226 Ma) and only the closure of the Palaeo-Asian Ocean, taking place during late Permian – Early Triassic time (Xiao *et al.* 2009), can match this. Nevertheless, the DSZZ granites have significantly lower Na_2O/K_2O ratios (0.96–1.25) than typical ocean slab-derived adakites (with Na_2O/K_2O ratios >2.3; Martin, 1999). Further, the evolved Sr ($^{87}Sr/^{86}Sr$ (226 Ma) ≥0.7042) and Nd ($^{143}Nd/^{144}Nd$ (226 Ma) ≤0.5119) isotopic compositions of the DSZZ granites contrast with MORB-like Sr–Nd isotopic compositions of slab melts interacted or not with overlying mantle wedge peridotite. The DSZZ granites were therefore not likely to originate from slab-melt–peridotite interaction.

Some studies have proposed that adakitic rocks can be generated by melting of hydrated mantle peridotite (Stern & Hanson, 1991; MacPherson, Dreher & Thirlwall, 2006) or AFC processes in basaltic magmas (e.g. Richards & Kerrich, 2007; Fu *et al.* 2012*b*). However, the SiO_2 (65.9–70.8 wt %), MgO (0.46–1.86 wt %) and Sr (458–1042 ppm) contents of the DSZZ granites are inconsistent with those of the low-SiO_2 adakites (<60 wt %, such as the sanukitoids described by Stern & Hanson, 1991), which have been suggested as a result of melting of peridotite source metasomatized by slab melts (Martin *et al.* 2005), but similar to those of the high-SiO_2 adakites. Derivation of hydrated mantle peridotite for the DSZZ granites is therefore impossible here. The EM1-like Sr–Nd isotopic features (Fig. 7a) of the DSZZ granites are similar to those of the coeval-enriched mantle-derived alkaline magma rocks (Yang *et al.* 2012; Zhang *et al.* 2012) and the Devonian Hongshila pyroxenite-hornblendite complex (Zhang *et al.* 2009*a*), and may be an indication that AFC processes play an important role in magma petrogenesis. Indeed, their Sr–Nd compositions could be modelled by EM1-derived melts with assimilation of 18 % crustal materials (represented by the intermediate granulite sample DMP-27; Liu *et al.* 2004) and a rate ratio of assimilation and fractional crystallization (*r*) close to 0.2. However, extremely low Sr/Nd ratios (Sr/Nd = 2.0; Table 3) are required in this model for the crustal contamination end-member. The required Sr/Nd ratios are obviously lower than the average Sr/Nd ratios of the continental crust (16.0) and LCC (31.6) recommended by Rudnick & Gao (2014), which makes the modelled results infeasible. Furthermore, the presence of mafic enclaves locally entrained by the DSZZ granites and granodiorites in field investigations contrasts with crustal assimilation because mafic enclaves are normally regarded as proof of basaltic injection into felsic melts (Xu *et al.* 2004; Yang *et al.* 2007) rather than crustal contamination. AFC processes in basaltic magmas can therefore also be ruled out.

Mixing of mafic and felsic magmas also have been proposed to account for some adakitic rocks (e.g. Guo *et al.* 2007; Streck, Leeman & Chesley, 2007). The local presence of pyroxenite and diorite enclaves in the DSZZ complex and adjacent Dushan complex implies basaltic injection into these magmas. This process probably resulted in the slightly elevated Magnesium number (such as sample HGY-2 with Mg no. of 51)

https://doi.org/10.1017/S0016756817000437 Published online by Cambridge University Press

and Cr contents. However, no reversely zoned plagioclase is observed in the petrographic study. Moreover, there is no obvious positive correlation between initial Nd isotopes and MgO and Cr contents. Such petrologic and geochemical characteristcis and the local occurrence of mafic enclaves possibly indicate that the addition of basaltic components does not play a significant role in magma petrogenesis. Although we cannot completely rule out this scenario, we do not favour it.

Preclusion of a mantle origin leads us to favour a crustal origin for the Triassic DSZZ granites. The adakitic characteristics of the DSZZ granites may have been generated by melting of thickened LCC that was delaminated or not (e.g. Atherton & Petford, 1993; Xu *et al.* 2002, 2006*a*; Gao *et al.* 2004), or just inherited from the crustal origin (Ma *et al.* 2012, 2015). In the former petrogenetic hypothesis, depletion in HREE and high Sr/Y without Eu anomalies are normally explained by deep melting (at depths >45 km) with the presence of garnet, amphibole, clinopyroxene and little or no plagioclase as stable and residual minerals (Atherton & Petford, 1993). The equilibrium *P*–*T* conditions estimates of the Palaeozoic kimberlites-hosted lower-crustal xenoliths in Fuxian County revealed that the depth of the lower boundary of the crust exceeded 30 km during early Palaeozoic time (Zheng *et al.* 2004*a*, *b*). The crust was then significantly thickened in the northern NCC by generally N–S-directed tectonic shortening during middle–late Permian time related to the assembly of the Mongolian composite terranes with the NCC (Zhang *et al.* 2011; Lin *et al.* 2013). Nevertheless, whether a Triassic-thickened LCC existed or not remains unknown.

Regardless of the thickness of the Mesozoic continental crust of the NCC, Ma *et al.* (2015) carried out trace-element modelling (with the depth ranging from ≤33 to >45 km) on the Mesozoic adakitic rocks from the northern part of the NCC, where the DSZZ granites are also located. We compared trace-element data with these modelled results. Most of the DSZZ granites samples can be generated either by 15–28 % melting of the mafic LCC of the NCC with residues of garnet-bearing granulite (33–40 km) or by approximately 50 % melting with residues of eclogite (>45 km) as indicated in the Sr/Y–Y diagram (Fig. 9a), and can be generated by 10–25 % melting with residues of garnet-bearing granulite as indicated in the $(La/Yb)_N$–Yb_N diagram (Fig. 9b). Hence, on the basis of trace-element features, the DSZZ granites can be produced either by low melt fractions with residues of garnet-bearing granulite (Cpx:Opx:Am:Grt:Pl:Ilm:Rt = 40:20:24:10:5:0.5:0.5) or by large melt fractions with residues of eclogite (Cpx:Grt:Rt = 70:29:1; Ma *et al.* 2015). However, according to the melting experiments on compounds with major elements analogous to mafic LCC estimated by Rudnick & Gao (2003) and Condie & Selverstone (1999), conducted by Qian & Hermann (2013), their major-element contents (such as SiO_2, MgO, Mg no., Al_2O_3, K_2O/Na_2O) are consistent with the experimental results of 15–22 % melting of mafic LCC at 800–950 °C and 10–12.5 kbar (corresponding to a depth of 30–40 km; experimental run C-3180; Fig. 9c–f). Increasing melting (such as 50 % melt proportions) will produce elevated CaO, MgO, Mg no. and Al_2O_3 and depressed SiO_2 and K_2O/Na_2O values (Winther, 1996; Qian & Hermann, 2013), which are inconsistent with the major elemental characteristics of the DSZZ granites. Although low melt proportions products at higher pressures (15 kbar; corresponding to a depth of >45 km) and low temperatures (800 °C; experimental run C-3171) would also display similar major element contents, it cannot produce appropriate Sr/Y, Y, $(La/Yb)_N$ and Yb values (Fig. 9a, b). Furthermore, $(Gd/Yb)_N$ values will be strongly elevated in melts coexisting with high proportions of amphibole and especially garnet (Wang *et al.* 2007; Qian & Hermann, 2013). As calculated by Ma *et al.* (2015), melts generated by 15–25 % melting with residues of eclogite will have $(Gd/Yb)_N$ values of 4.1–4.3. These values are obviously higher than those ($(Gd/Yb)_N$ = 2.8–3.9) of the DSZZ granites. Additionally, the EM1-like Sr–Nd isotopic compositions of the DSZZ granites are very different when compared to those of melts produced by foundered lower crust followed by interaction with mantle peridotites (Fig. 7a; Xu *et al.* 2002; Gao *et al.* 2004). We therefore conclude that melting of thickened or foundered LCC cannot be used to explain the petrogenesis of the DSZZ granites. Their adakitic characteristics may simply be inherited from the mafic LCC of the NCC (with residues of garnet-bearing granulite at depths of 33–40 km).

As discussed above, the DSZZ granites have Sr/Y and Y values and major-element contents similar to melts coexisting with garnet-bearing granulite/or mafic LCC by approximately 15–28 % melting proportions (Fig. 9a, b). Moreover, their Zr (148–217 ppm) and Hf (4.8 ppm) are also consistent with those (Zr = 185–232 ppm and Hf = 4.3–5.1 ppm; Ma *et al.* 2015) of melts coexisting with garnet-bearing granulite. Depletion in Nb–Ta and Ti was considered to be inherited from the intrinsic characteristics of the LCC of the NCC (Rudnick & Gao, 2003, 2014; Ma *et al.* 2015), and does not necessarily indicate high-pressure melting conditions. However, some previous studies have argued that garnet is not a common mineral in the lower crustal xenoliths (e.g. Ma *et al.* 2012). Here, we argue that this cannot be used to exclude the possibility that small proportions of garnet (≤10 %) could have existed in the mafic LCC, because garnet is present in the deep-seated crustal xenoliths from Fuxian and Hannuoba (Liu *et al.* 2004; Zheng *et al.* 2004*a*). Distinctive high-K_2O (3.8–4.7 wt %) features also can be observed. This may be related to incorporation of some enriched subcontinental lithospheric mantle-derived materials into the LCC prior to melting (Roberts & Clemens, 1993). We therefore suggest the pre-existing ancient mafic LCC of the NCC as the main source for the DSZZ granites.

The EM1-like Sr–Nd isotopic features of the DSZZ granites (Fig. 7a) could be produced by either enriched

https://doi.org/10.1017/S0016756817000437 Published online by Cambridge University Press

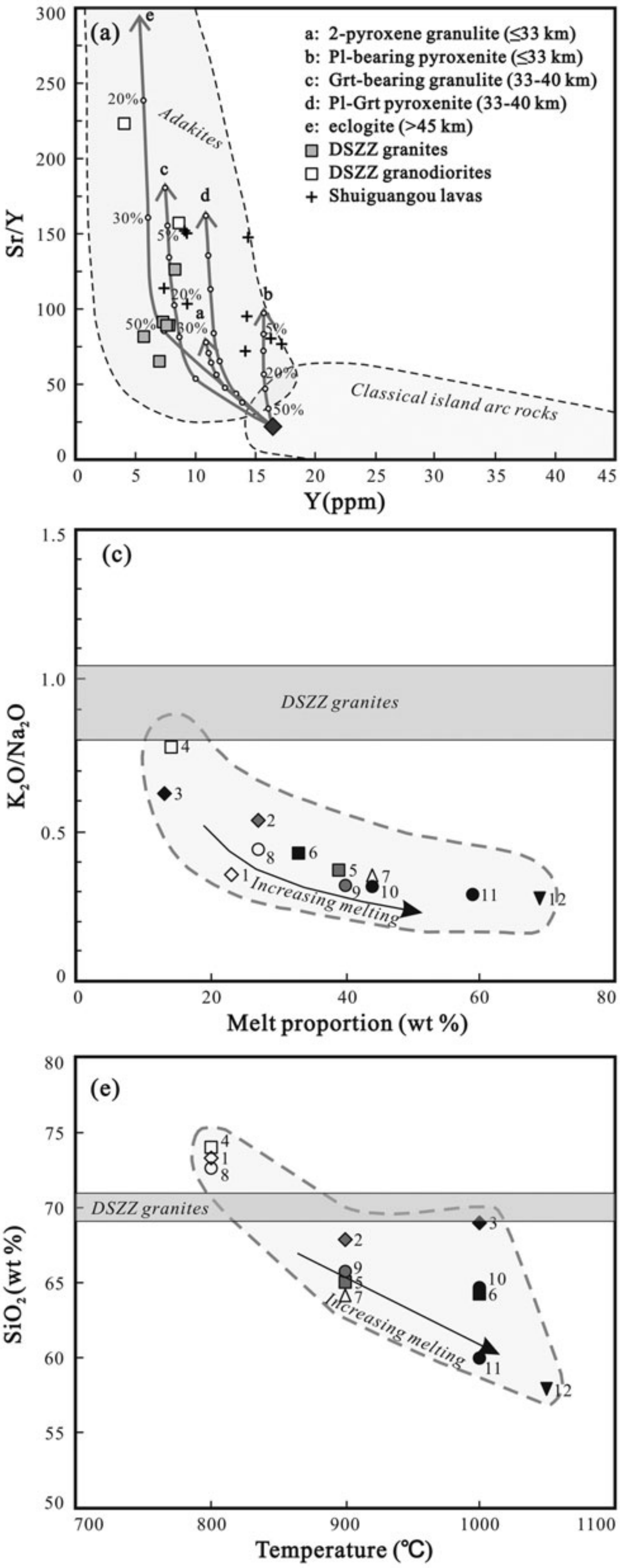

Figure 9. Plot of (a) Sr/Y v. Y, (b) $(La/Yb)_N$ v. Yb_N, (c) K_2O/Na_2O v. melt proportion, (d) Al_2O_3 v. pressure, and (e) SiO_2 and (f) Mg no. v. melt temperature. Data for the DSZZ granodiorites (Ye *et al*. 2014) and the Shuiquangou lavas (Ma *et al*. 2012) are also shown. Partial melting curves for batch melting of the mafic lower crust of the NCC in (a) and (b) are from Ma *et al*. (2015), and the fields of adakites and classical island-arc rocks (andesite-dacite-rhyolite) are modified from Defant & Drummond (1990). In the partial melting model, the assumed starting material is represented by the weighted average of Archean mafic-granulite terrains and mafic lower-crustal xenoliths in Phanerozoic basalts and kimberlites. For more details see Ma *et al*. (2015). Experimental melting data and its trends for major element values in (c–f) are from Qian & Hermann (2013). Numbers labelled adjacent to each symbol correspond to different experiment runs.

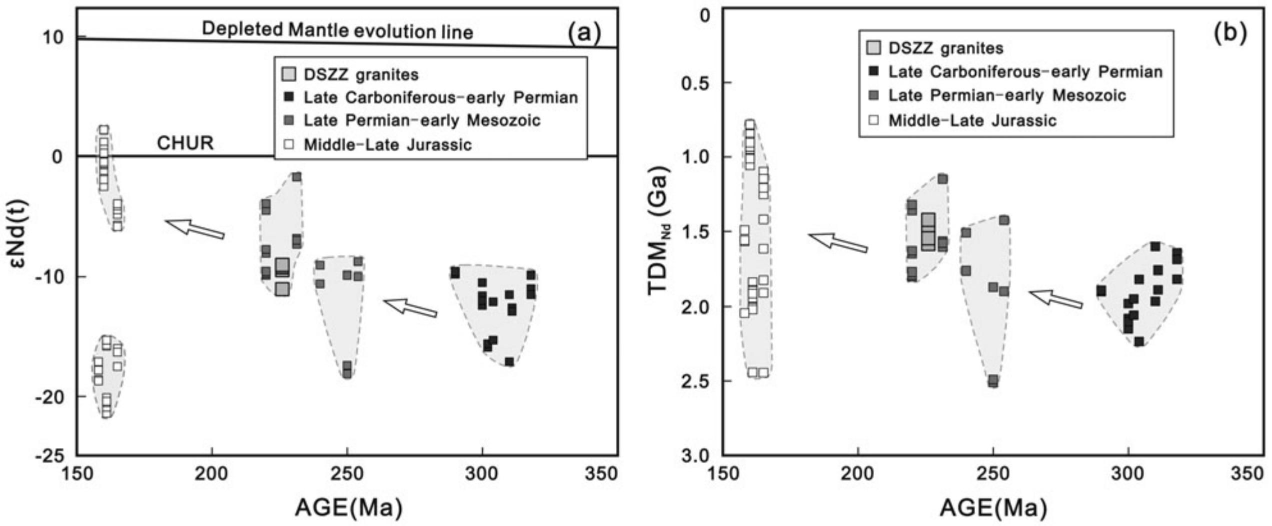

Figure 10. Plots of (a) $\varepsilon_{Nd}(t)$ and (b) TDM_{Nd} v. U–Pb age for the Dashizhuzi granites. Data for the late Carboniferous – early Permian intermediate-felsic magma rock are from Wang *et al*. (2009) and Zhang *et al.* (2009*b*) . Data for the late Permian – early Mesozoic intermediate-felsic magma rocks are from Wang *et al*. (2009), Zhang *et al.* (2009*b*), Ma *et al*. (2012), Xiong *et al.* 2017; and this study. Data for the Middle–Late Jurassic intermediate-felsic magma rocks are from Gao *et al*. (2004) and Zhang, Yuan & Wilde (2014).

lithospheric mantle or LCC. As mentioned above, pure mantle derivation can be ruled out, and the addition of basaltic components plays a limited role in magma petrogenesis. Moreover, the DSZZ granites have Sr–Nd isotopic compositions plotting in the field of the Mesozoic lower crustal granulite xenoliths (Liu *et al*. 2004; She *et al*. 2006) and cumulates (Shao *et al*. 2006). Old Nd model ages (TDM_{Nd} (226 Ma) = 1.42–1.58 Ga) also indicate ancient crustal materials were involved in the magma source, which is consistent with the interpretation indicated by their major- and trace-element characteristics.

In addition, variable *in situ* Hf isotopic compositions (with ε_{Hf} (226 Ma) up to –1.4) and young Hf (TDM_{Hf} (226 Ma) = 0.95–1.36 Ga) model ages suggest that a primitive component was involved in the magma source. The incorporation of mantle component is also indicated by the systematic changes in Nd and Hf isotopic compositions of the late Palaeozoic – Jurassic intermediate-felsic magma rocks in the northern NCC. The early Mesozoic intermediate-felsic magma rocks have higher $\varepsilon_{Nd}(t)$, $\varepsilon_{Hf}(t)$ values and younger Nd, Hf model ages than their late Palaeozoic counterparts (Figs 10, 11). This primitive component was probably derived from the subcontinental lithospheric mantle in an extensional environment, as there are widespread contemporaneous lithospheric mantle-derived alkaline magma rocks (e.g. Yan *et al*. 2000; Mu *et al*. 2001; Han, Kagami & Li, 2004; Yang *et al*. 2012; Zhang *et al*. 2012) along the northern margin of the NCC. Incorporation of subcontinental lithospheric mantle-derived materials into the LCC therefore led to the formation of a juvenile lower-crust component during early Mesozoic time, and melting of the mixture of ancient and juvenile lower-crustal materials resulted in the relatively high Nd and Hf isotopic compositions of the DSZZ granites.

Depletion in P may result from apatite separation. Depletion in Ti is mainly related to the intrinsic characteristics of the LCC of the NCC, and may be partly related to fractionation of titanite (a common accessory mineral in the DSZZ granites). However, no clear negative correlation is observed in the plot of Ba/Sr v. δEu (online Supplementary Figure S2, available at http://journals.cambridge.org/geo), which indicates that no significant plagioclase separation occurred. In summary, the petrography, geochemistry and isotope compositions suggest that the DSZZ granites were derived directly from melting of mixed lower-crust sources, which consisted of pre-existing ancient crustal and juvenile crustal materials, followed by fractionation of apatite and titanite.

6.c. Source of lamprophyre dykes

6.c.1. Crustal contamination

It is important to evaluate whether these lamprophyre dykes have undergone significant crustal contamination and magmatic differentiation before trying to explore their mantle sources. They seem to have experienced significant crustal contamination as indicated by their 'crustal-like' geochemical features (e.g. depletion in HFSE and enrichment in Pb; Fig. 6c). However, the Group 2 dykes have primitive Mg no. (76–77; Table 1), Cr (563–712 ppm), Co (360–470 ppm) and Al_2O_3 (11.7–12.4 wt %) values, which could be regarded as the mantle-derived primary or near-primary melts. Their Ba (1989–2293 ppm) and Sr (1004–1011 ppm) contents are apparently different from those of the average continental crust (456 ppm Ba; 320 ppm Sr; Rudnick & Gao, 2014), suggesting that trace elements were not obviously contaminated by crustal materials. Moreover, $^{87}Sr/^{86}Sr$ and

https://doi.org/10.1017/S0016756817000437 Published online by Cambridge University Press

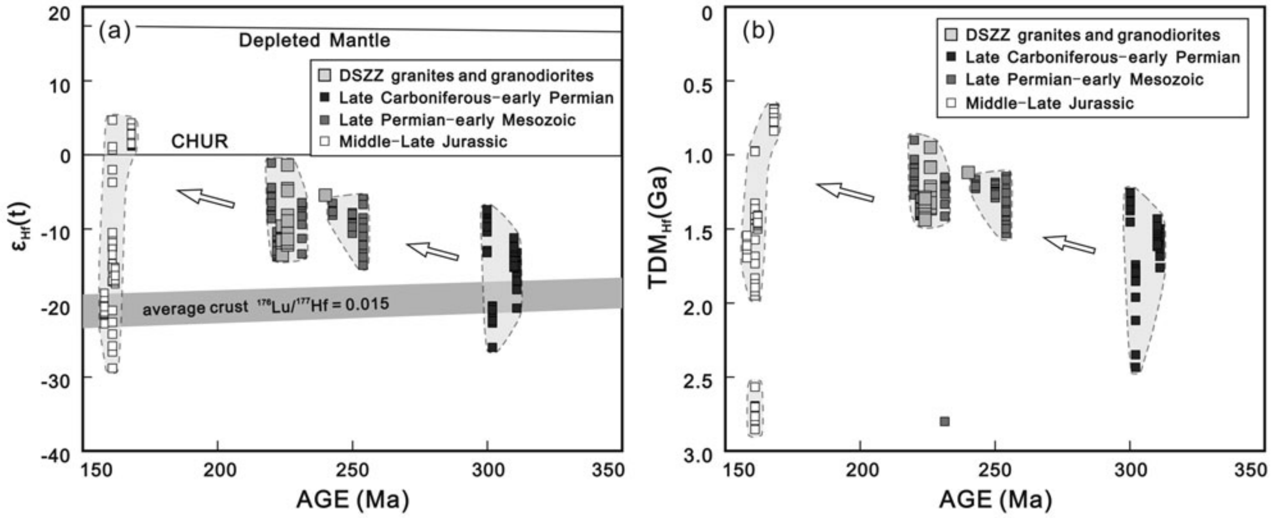

Figure 11. Plots of (a) $\varepsilon_{Hf}(t)$ and (b) TDM_{Hf} v. U–Pb age for the Dashizhuzi granites. Data sources as for Figure 10.

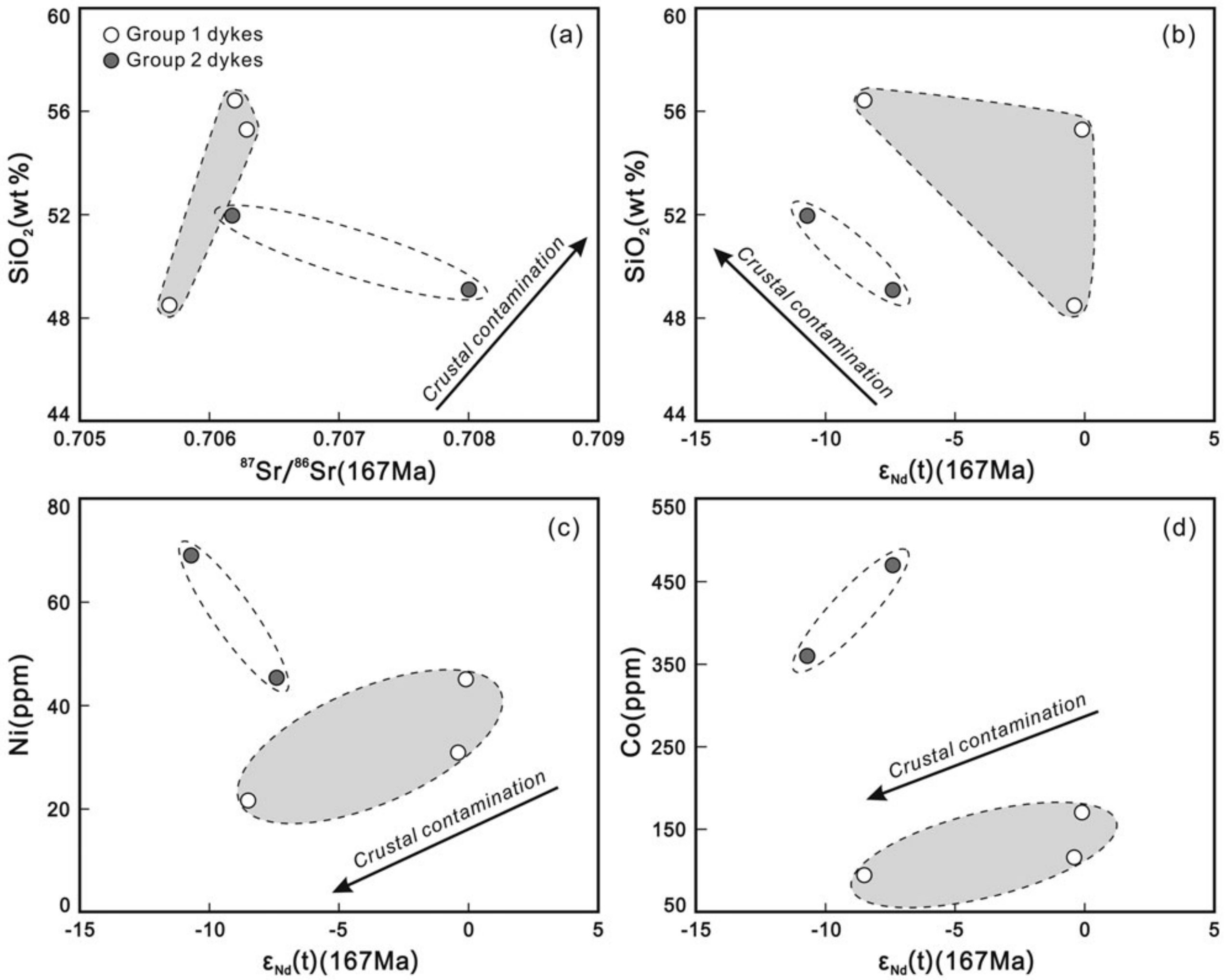

Figure 12. Plots of (a) $^{87}Sr/^{86}Sr$ v. SiO_2 and (b–d) $\varepsilon_{Nd}(t)$ versus SiO_2, Ni and Co for the lamprophyre dykes.

$\varepsilon_{Nd}(t)$ values decrease with increasing SiO_2 contents (Fig. 12a, b); such characteristics are also inconsistent with crustal contamination and may simply reflect a heterogeneous mantle source. Although there are some inherited Archean–Palaeoproterozoic zircons present in the sample SCYM-2, given the fact that less than 70 zircon grains were picked out from *c.* 9 kg of rocks, crustal contamination played a limited role in the magma petrogenesis. Crustal contamination is therefore negligible.

Similarly, high Mg no. (62–71), Cr (174–461 ppm) and Co (51–171 ppm) and low SiO_2 (48.5–56.4 wt %)

https://doi.org/10.1017/S0016756817000437 Published online by Cambridge University Press

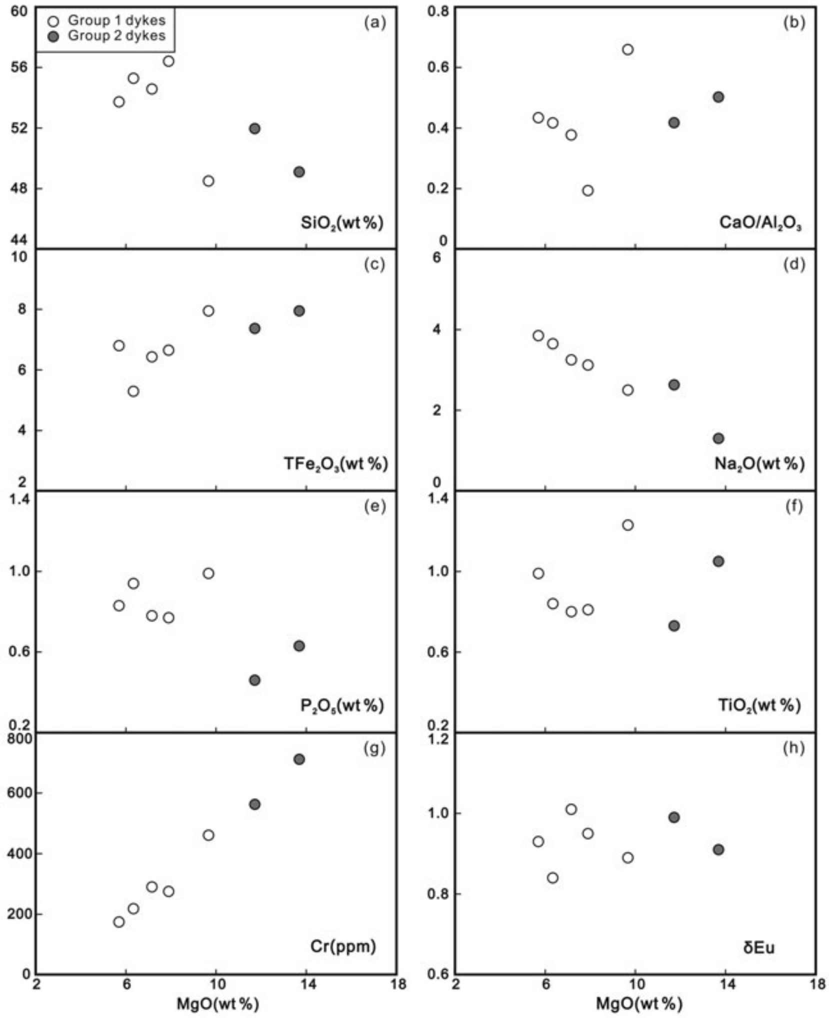

Figure 13. Plots of MgO v. selected major and trace elements for the lamprophyre dykes.

values of the Group 1 dykes also suggest that they are dominantly mantle derived. Slightly positive correlations between $\varepsilon_{Nd}(t)$ and compatible elements (e.g. Ni, Co and Cr; Fig. 12c, d) are observed, which indicates that some extent of crustal contamination was involved in the magma evolution processes. Incorporation of some crustal materials is also suggested by the occurrence of a large range of zircon populations (Fig. 3c). Bulk crustal contamination is impossible however, given the fact that only about 120 zircon grains were picked out from *c.* 11 kg of rocks. In addition, their Ba (1557–3289 ppm) and Sr (849–1673 ppm) contents are much higher than those of the average continental crust (Rudnick & Gao, 2014). Nb/U (1.7–4.0) and Ce/Pb (11.7–27.3) ratios are also different from those of the average continental crust (6.2 Nb/U; 3.9 Ce/Pb; Rudnick & Gao, 2014). The Group 1 dykes have therefore experienced low extent rather than bulk crustal contamination.

6.c.2. *Fractional crystallization*

The Group 2 dykes have linear correlations between MgO and major and trace elements, although we do not have many samples (Fig. 13). $^{T}Fe_2O_3$, CaO/Al_2O_3 and Cr increase and SiO_2 decreases with increasing MgO contents; such characteristics indicate that the Group 2 dykes may have experienced some fractionation of olivine and clinopyroxene. Similarly, positive correlations between P_2O_5, TiO_2 and MgO indicate that some fractionation of accessory minerals (e.g. apatite and Fe–Ti oxides) may have occurred. In addition, the absence of Eu and Sr anomalies suggest that fractionation of plagioclase is insignificant.

The Group 1 dykes do not have clear linear correlations between MgO and major and trace elements (Fig. 13). The parental magma may not have experienced extensive fractional crystallization. Likewise, the absence of Eu and Sr anomalies indicates that plagioclase was not a significant fractionating phase.

6.c.3. *Source of Group 2 dykes*

The Group 2 dykes have primitive Mg no. (76–77), Cr (563–712 ppm), Co (360–470 ppm) and Al_2O_3 (11.7–12.4 wt%) values, which are similar to the features of mantle-derived primary or near-primary melts. These lamprophyre dykes could therefore originate from

https://doi.org/10.1017/S0016756817000437 Published online by Cambridge University Press

either the convective asthenospheric mantle or the subcontinental lithospheric mantle. The high Ba/Th (237–364) and low Ce/Pb (7.4–8.5) and Nb/U (5.0–6.0) ratios are obviously different from those of the MORB (Ba/Th = 86; Ce/Pb = 22.4; Nb/U = 45.7; Salters & Stracke, 2004). Moreover, their enriched Sr–Nd isotopic compositions and ancient TDM_{Nd} age (1.68–2.82 Ga) also argue against an asthenospheric mantle derivation. Due to the limited role of crustal contamination as discussed above, negative Nb–Ta and positive Pb anomalies further demonstrate that the Group 2 dykes cannot be generated from melting of asthenospheric mantle. Asthenospheric mantle derivation can therefore be ruled out, and the subcontinental lithospheric mantle may account for the petrogenesis of the Group 2 dykes.

Distinct geochemical features, such as strong fractionation between LREE and HREE, LILE enrichment and HFSE depletion, are similar to those of some Mesozoic mafic dykes in the northern NCC (Jiang *et al*. 2010; Fu *et al*. 2012*a*; Duan *et al*. 2014) and in the Jiaodong Peninsula (Ma *et al*. 2014*a*, *b*), interpreted to have been derived from an enriched lithospheric mantle. The enriched Sr–Nd isotopic compositions of the Group 2 dykes are also similar to those of the early Mesozoic enriched lithospheric mantle-derived alkaline magma rocks (Fig. 7b; e.g. Yan *et al*. 2000; Yang *et al*. 2012; Zhang *et al*. 2012). Mantle enrichment was probably produced by subduction processes as indicated by the depletion of HFSE (e.g. Nb, Ta, Zr and Hf) relative to neighbouring elements in the primitive mantle-normalized pattern (e.g. Duggen *et al*. 2005; Ma *et al*. 2014*a*). Moreover, the enrichment of the mantle source probably occurred during ancient time, which is suggested by the ancient whole-rock TDM_{Nd} ages (1.68–2.82 Ga) of the Group 2 dykes. The TDM_{Nd} ages are roughly consistent with the original formation (Archean; e.g. Wu *et al*. 2006*b*; Zhang *et al*. 2008; Liu *et al*. 2015) and replacement (late Palaeoproterozoic; Gao *et al*. 2002; Liu *et al*. 2011, 2012, 2015) age of the subcontinental lithospheric mantle beneath the NCC. The Group 2 dykes were therefore derived from an ancient subcontinental lithospheric mantle.

The high K_2O content and enrichment of LILE suggest that K and volatile-bearing minerals such as phlogopite or amphibole were present in the mantle source of the Group 2 dykes. Their moderate Ba/Rb (14–29) and Rb/Sr (0.07–0.16) ratios indicate that the potassic phase in the magma source may be either phlogopite or amphibole (Fig. 14a). The identification of phlogopite and/or amphibole in the source region of the Group 2 dykes implies that mantle metasomatism by fluids or volatile-rich melts occurred prior to melting (Jiang *et al*. 2010). In addition, the K/Yb and Dy/Yb ratios have been proposed to provide constraint on the composition of the mantle source and melt proportion (Duggen *et al*. 2005). The Group 2 dykes have Dy/Yb ratios of 2.37–3.21 and plot in the field of garnet-facies lherzolite (Fig. 14b), which suggests that some proportions of garnet are present in the source of the Group 2 dykes. The occurrence of garnet in the magma source is also consistent with their high $(La/Yb)_N$ and $(Gd/Yb)_N$ values (30–40 and 4.0–5.7). The Group 2 dykes were therefore probably derived from a garnet-facies phlogopite and/or amphibole-bearing lherzolite lithospheric mantle.

6.c.4. Source of Group 1 dykes

High Mg no. (62–71), Cr (174–461 ppm) and Co (51–171 ppm) and low SiO_2 (48.5–56.4 wt %) values of the Group 1 dykes also suggest a dominantly mantle derivation. Although the Group 1 dykes have experienced a low extent of crustal contamination, the LILE enrichment and HFSE depletion observed in the most basic dyke sample (SCYM-16) indicates a dominantly subduction-related metasomatized lithospheric mantle derivation. Their relatively lower MgO and compatible trace-element (such as Cr, Co and Ni) contents than the Group 2 dykes probably call for a relatively fertile mantle source. Dyke samples SCYM-5 and SCYM-16 have nearly primitive Nd isotopes (Fig. 7b), suggesting that a depleted component (e.g. asthenospheric mantle) was incorporated in the magma origin. This is supported by their identical Sr–Nd isotopic characteristics with those of the Triassic Hongqiling-Piaohechuan mafic-ultramafic rocks (Wu *et al*. 2004) and the Late Jurassic Xinglonggou lavas (Gao *et al*. 2004), which were thought to be derived from asthenospheric mantle or to have an asthenospheric mantle component. The relatively young TDM_{Nd} ages (0.93–1.51 Ga) is also consistent with the involvement of depleted component in the magma source. Moreover, the Group 1 dykes have Th/U (3.3–3.8, except SCYM–5), Ba/Th (53–180) and Ce/Pb (11.7–27.3; Table 1) ratios similar to those (Th/U = 3.3; Ba/Th = 86; Ce/Pb = 22.4; Salters & Stracke, 2004) of the MORB. Furthermore, the significantly higher REE contents of the Group 1 dykes (Fig. 6c, d) compared to the Group 2 dykes probably suggests that the incorporated depleted mantle materials are probably asthenospheric mantle-derived, volatile-rich, low-density melts. The Group 1 dykes were therefore derived from an ancient subcontinental lithospheric mantle with incorporation of asthenospheric mantle-derived melts.

As discussed above, the Group 1 dykes have experienced a low extent of crustal contamination. However, their variable ε_{Nd} (167 Ma) values (–8.5 to –0.1) cannot be produced through crustal contamination, because the Group 1 dykes have significantly higher Sr (849–1673 ppm) and Nd (76–128 ppm) contents than the average continental crust (320 ppm Sr; 20 ppm Nd; Rudnick & Gao, 2014). Their Sr–Nd compositions are therefore insensitive to crustal contamination, and lowering the ε_{Nd} values by 7.5 units requires bulk crustal contamination. The variation in ε_{Nd} (167 Ma) values therefore cannot be caused by assimilation of crustal materials; such characteristics may reflect heterogeneity in the magma source, which was

https://doi.org/10.1017/S0016756817000437 Published online by Cambridge University Press

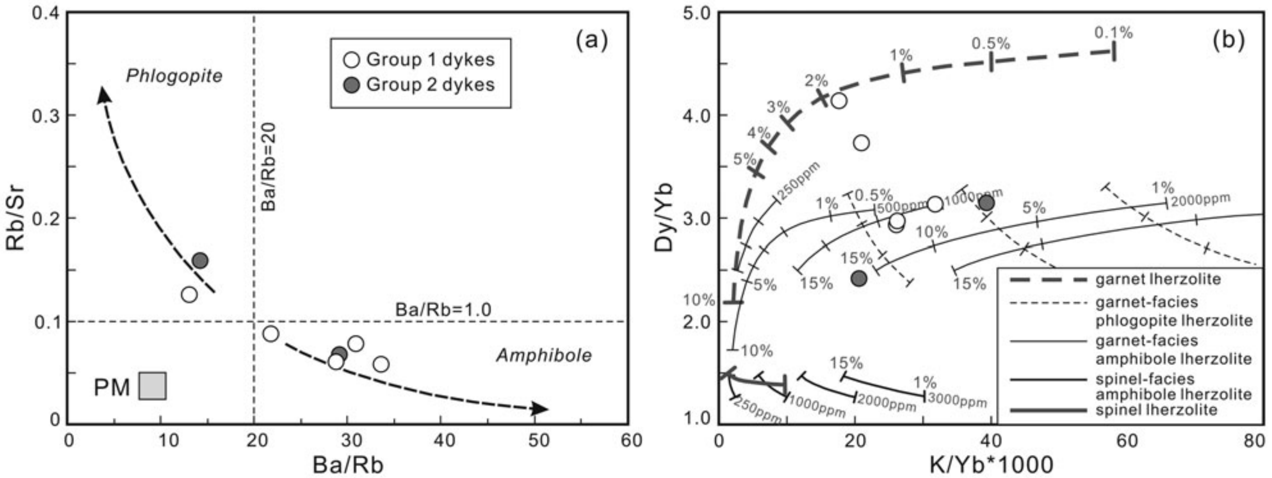

Figure 14. (a) Plots of Ba/Rb v. Rb/Sr (modified after Furman & Graham, 1999; Ma *et al.* 2014*a*) and (b) K/Yb v. Dy/Yb for the lamprophyre dykes. Melting curves of garnet lherzolite, garnet-facies phlogopite lherzolite, garnet-facies amphibole lherzolite, spineal-facies amphibole lherzolite and spinel lherzolite are from Duggen *et al.* (2005).

probably produced by variable degrees of mixing between the ancient subcontinental lithospheric mantle and asthenospheric mantle-derived component.

In addition, the high K_2O and Ba/Rb (13–34, most >21) and low Rb/Sr (0.06–0.13, most <0.10) values indicate that amphibole is the dominantly potassic phase in the mantle source (Fig. 14a). Such characteristics imply mantle metasomatism prior to melting. Additionally, the Group 1 dykes have Dy/Yb ratios ranging over 2.93–4.14, and plot in the field of garnet-facies amphibole lherzolite (Fig. 14b). Significantly high $(La/Yb)_N$ and $(Gd/Yb)_N$ values (36–92 and 5.8–8.8) further support the existence of garnet as a residual phase in the magma source. The Group 1 dykes were therefore probably derived from a garnet-facies amphibole-bearing lherzolite lithospheric mantle with incorporation of asthenospheric mantle-derived melts prior to melting.

6.d. Evolution of the lithosphere

Continental adakitic rocks are normally considered as a geodynamic indicator of crustal thickening, orogenic collapse and lithospheric delamination (e.g. Kay, 1978; Atherton & Petford, 1993; Xu *et al.* 2002; Ma *et al.* 2015). Interpretation of the Mesozoic adakitic rocks as resultants of crustal thickening have inferred the Late Mesozoic lithospheric delamination and destruction of the NCC (Xu *et al.* 2002; Gao *et al.* 2004). Ma *et al.* (2015) pointed out the flaw of this interpretation, and ascribed it to ignoring the effect of source composition on the generation of continental adakitic rocks. As discussed above, the Triassic DSZZ granites were produced from melting of mafic LCC, with residues of garnet-bearing granulite, at a normal continental crustal depth of 33–40 km. The adakitic characteristics were dominantly inherited from the protolith sources. Trace-element modelling also suggested that the melting depth required to produce the Jurassic adakitic rocks in the Yanshan belt is from <33 to 40 km (Ma *et al.* 2015). These lines of evidence therefore do not support the existence of a thickened mafic LCC during early Mesozoic time. The occurrence of these early Mesozoic adakitic rocks cannot be regarded as crucial evidence for later lower-crust foundering as an important mechanism for destruction of the NCC.

Mantle xenoliths entrained by Cenozoic volcanic rocks have distinct chemical compositions and ages compared to those entrained by Ordovician kimberlites, which suggested significant thinning and replacement of the lithospheric mantle beneath the eastern NCC during Mesozoic time (e.g. Griffin *et al.* 1998; Gao *et al.* 2002; Wu *et al.* 2006*b*; Chu *et al.* 2009; Liu *et al.* 2015). More than 100 km of ancient refractory lithospheric mantle beneath the NCC have been removed and replaced by young and fertile mantle materials (e.g. Menzies *et al.* 2007). However, when and how the replacement occurred has been debated for a long time (e.g. Xu, 2001; Gao *et al.* 2002; Zhang *et al.* 2002; Chen, Jahn & Zhai, 2003; Xu *et al.* 2006*b*, 2009; Liu *et al.* 2011, 2015; Fu *et al.* 2012*a*).

As discussed above, the Group 2 lamprophyre dykes were generated by a garnet-facies metasomatized lherzolite lithospheric mantle. Previous studies have proposed that the depth of garnet-facies zone in the upper mantle is greater than 75–85 km (e.g. McKenzie & O'Nions, 1991; Robinson & Wood, 1998; Klemme & O'Neill, 2000). The thickness of the Middle Jurassic (167 Ma) lithosphere beneath the Yanshan belt is therefore ≥75–85 km. The ancient Nd model ages of the Group 2 lamprophyre dykes suggest that the original Archean and Proterozoic lithospheric mantle has been preserved, and their chemical composition has not been changed at that time.

However, a petrogenetic study of the Group 1 lamprophyre dykes indicates a relatively fertile lithospheric mantle source that has experienced variable degrees of asthenospheric mantle-derived melt–peridotite interaction. Their significantly higher $(La/Yb)_N$ and $(Gd/Yb)_N$ values indicate a higher

https://doi.org/10.1017/S0016756817000437 Published online by Cambridge University Press

content of garnet in the source. It may therefore reflect an even greater melting depth than the Group 2 lamprophyre dykes. Previous studies have suggested that a change in magma source from lithospheric mantle to asthenospheric mantle and the occurrence of asthenosphere-derived magmas can be considered as an indicator of lithospheric thinning (e.g. Xu, 2006; Wu *et al*. 2008; Xu *et al*. 2009; Ma *et al*. 2014*a*).

The widespread early Mesozoic (240–220 Ma) alkaline magmas were considered to have enriched subcontinental mantle sources beneath the northern NCC (e.g. Yan *et al*. 2000; Mu *et al*. 2001; Han, Kagami & Li, 2004; Yang *et al*. 2012; Zhang *et al*. 2012). Studies of Triassic granitic igneous rocks also have suggested incorporation of variable amounts of subcontinental lithospheric mantle-derived materials in their origin (Figs 10, 11; e.g. Ma *et al*. 2012; Xiong *et al*. 2017; this study). Although some asthenospheric mantle components were considered to have been invoked in certain Triassic ultramafic-mafic igneous rocks (Tian *et al*. 2007; Fu *et al*. 2012*a*), this scenario is not common at that time. Asthenospheric mantle therefore does not have a significant role in the petrogenetic processes of the early Mesozoic magma rocks.

During Middle–Late Jurassic time large amounts of mafic to felsic magmas were emplaced in the northern NCC, including the Yanshan belt and Liaodong peninsula (e.g. Gao *et al*. 2004; Zhang *et al*. 2010*b*; Zhu, Yang & Wu, 2012; Zhang, Yuan & Wilde, 2014; this study). Geochemical data reveal significant involvement of asthenospheric mantle materials in these magmas, and their trace-element signatures are intermediate between clearly defined lithospheric and asthenospheric characteristics. Such characteristics probably suggest some extent of lithospheric thinning during Middle–Late Jurassic time, which was possibly induced by the subduction of the Palaeo-Pacific Plate beneath the Eurasian continent (e.g. Xu *et al*. 2013). Based on the petrogenetic processes of the Group 1 lamprophyre dykes in this study, melt–peridotite interaction processes probably played an important role in the change of chemical compositions of the lithospheric mantle beneath the northern part of the NCC. It has been demonstrated that melt–peridotite interaction can change rheology and modal composition of mantle rocks (Kelemen, Dick & Quick, 1992; Xu, 2001). Repeated invasion of a small amount of asthenosphere-derived volatile-rich melts would accumulate at the lithosphere–asthenosphere interface, and provide heat to cause melting of this zone and its gradual upwards movement (McKenzie, 1989). Meanwhile, upwelling of asthenosphere would lead to thermal weakening on the base of the lithospheric mantle. The melt–peridotite interaction and thermo-mechanical erosion may be jointly associated, rather than mutually exclusive (Xu, 2001). The mechanism of lithospheric thinning is therefore mainly by coupled melt–peridotite interaction and thermo-mechanical erosion during Middle Jurassic time. Although the Late Jurassic Xinglonggou lavas were considered to have been produced as a result of lower crustal foundering (Gao *et al*. 2004), the influence of lower crustal foundering may be local and limited. One reason is that the Jurassic adakitic rocks in the Yanshan belt were produced at a depth from <33 to 40 km (Ma *et al*. 2015); such an interpretation does not support the existence of thickened mafic LCC during Jurassic time. Another reason is that the original Archean and Proterozoic lithospheric mantle has been preserved, according to the petrogenetic study of Group 2 lamprophyre dykes. If lower crustal foundering has occurred, the original Archean and Proterozoic lithospheric mantle would have detached into the asthenosphere, accompanied by formation of juvenile lithosphere.

In summary, thinning of the early Mesozoic lithospheric mantle beneath the northern part of the NCC was dominantly though coupled melt–peridotite interaction and thermo-mechanical erosion prior to Middle Jurassic time. The chemical compositions were modified at the bottom of the lithospheric mantle through melt–peridotite interaction processes. However, whether a rapid removal process occurred at some point after Middle Jurassic time remains the topic for further studies.

7. Conclusions

Integrated U–Pb geochronology, elemental and Sr–Nd–Pb isotope studies of the DSZZ granites and lamprophyre dykes in the northern NCC allow us to make the following conclusions.

(1) The DSZZ granites are dated at 226 ± 3 Ma. The occurrence of voluminous Triassic alkaline, mafic-ultramafic and felsic magma rocks along the northern margin of the NCC suggests a pronounced magmatism period during Middle Triassic time.

(2) The Triassic DSZZ granites were produced from melting of mafic LCC of the NCC with residues of garnet-bearing granulite at normal continental crustal depths of 33–40 km, followed by fractionation of apatite and titanite. Their protolith source consists of pre-existing ancient crustal and lithospheric mantle-derived juvenile crustal materials.

(3) The Group 2 lamprophyre dykes were derived from an ancient garnet-facies phlogopite and/or amphibole-bearing lherzolite lithospheric mantle at depths greater than 75–85 km. However, the Group 1 lamprophyre dykes have a relatively fertile lithospheric mantle source (garnet-facies amphibole-bearing lherzolite) that has experienced variable degrees of asthenospheric mantle-derived melt–peridotite interaction prior to melting. The melting depth of the Group 1 lamprophyre dykes is even greater than the Group 2 lamprophyre dykes.

(4) Thinning of late Mesozoic lithospheric mantle beneath the northern part of the NCC is dominantly thought to have occurred via coupled melt–peridotite interaction and thermo-mechanical erosion prior to Middle Jurassic time. The chemical compositions were

modified at the bottom of the lithospheric mantle through melt–peridotite interaction processes.

Acknowledgements. This study was financially supported by the Science and Technology Programme of Fujian, China (Grant DK2015001). J. P. Lu is thanked for his help with the petrographic study. Y. Y. Zhang and Y. L. Zhai are acknowledged for their help with the LA-ICP-MS dating. We are also grateful to C. Chen and the Rixing Mining Co. Ltd., Lingyuan for the assistance with fieldwork. Finally, we thank the reviewer Jingao Liu and two anonymous reviewers for their constructive comments on this manuscript.

Supplementary material

To view supplementary material for this article, please visit https://doi.org/10.1017/S0016756817000437

References

ATHERTON, M. P. & PETFORD, N. 1993. Generation of sodium-rich magmas from newly underplated basaltic crust. *Nature* **362**, 144–6.

BLICHERT-TOFT, J., CHAUVEL, C. & ALBARÈDE, F. 1997. Separation of Hf and Lu for high-precision isotope analysis of rock samples by magnetic sector-multiple collector ICP-MS. *Contributions to Mineralogy and Petrology* **127**, 248–60.

BOUVIER, A., VERVOORT, J. D. & PATCHETT, P. J. 2008. The Lu–Hf and Sm–Nd isotopic composition of CHUR: constraints from unequilibrated chondrites and implications for the bulk composition of terrestrial planets. *Earth and Planetary Science Letters* **273**, 48–57.

CHEN, B., JAHN, B. M. & ZHAI, M. G. 2003. Sr–Nd isotopic characteristics of the Mesozoic magmatism in the Taihang-Yanshan orogen, North China Craton, and implications for Archaean lithosphere thinning. *Journal of the Geological Society* **160**, 963–70.

CHU, Z. Y., WU, F. Y., WALKER, R. J., RUDNICK, R. L., PITCHER, L., PUCHTEL, I. S., YANG, Y. H. & WILDE, S. A. 2009. Temporal evolution of the lithospheric mantle beneath the eastern North China Craton. *Journal of Petrology* **50**, 1857–98.

CONDIE, K. C. & SELVERSTONE, J. 1999. The crust of the Colorado Plateau: new views of an old arc. *Journal of Geology* **107**, 387–97.

DEFANT, M. J. & DRUMMOND, M. S. 1990. Derivation of some modern arc magmas by melting of young subducted lithosphere. *Nature* **347**, 662–5.

DRUMMOND, M. S. & DEFANT, M. J. 1990. A model for trondhjemite-tonalite-dacite genesis and crustal growth via slab melting: Archean to modern comparisons. *Journal of Geophysical Research* **95**, 21503–21.

DU, J. J., MA, Y. S., ZHAO, Y. & WANG, Y. B. 2007. SHRIMP U–Pb zircon dating of the Yiwulüshan granite in western Liaoning and its geological implications. *Geology in China* **34**, 26–33 (in Chinese with English Abstract).

DUAN, X. X., ZENG, Q. D., YANG, J. H., LIU, J. M., WANG, Y. B. & ZHOU, L. L. 2014. Geochronology, geochemistry and Hf isotope of Late Triassic magmatic rocks of Qingchengzi district in Liaodong peninsula, Northeast China. *Journal of Asian Earth Sciences* **91**, 107–24.

DUGGEN, S., HOERNLE, K., BOGAARD, P. V. & GARBE-SCHÖNBERG, D. 2005. Post-collisional transition from subduction to intraplate-type magmatism in the westernmost Mediterranean: evidence for continental-edge delamination of subcontinental lithosphere. *Journal of Petrology* **46**, 1155–201.

FU, L. B., WEI, J. H., KUSKY, T. M., CHEN, H. Y., TAN, J., LI, Y. J., KONG, L. J. & JIANG, Y. J. 2012a. Triassic shoshonitic dykes from the northern North China Craton: petrogenesis and geodynamic significance. *Geological Magazine* **149**, 39–55.

FU, L. B., WEI, J. H., KUSKY, T. M., CHEN, H. Y., TAN, J., LI, Y. J., SHI, W. J., CHEN, C. & ZHAO, S. Q. 2012b. The Cretaceous Duimiangou adakite-like intrusion from the Chifeng region, northern North China Craton: crustal contamination of basaltic magma in an intracontinental extensional environment. *Lithos* **134–5**, 273–88.

FU, L. B., WEI, J. H., WEI, Q. R., TAN, J., LI, Y. J., LI, Y. H., WANG, M. Z. & JIANG, Y. J. 2010. Petrogenesis and geodynamic setting of Late Triassic dykes of Jinchanggouliang, eastern Inner Mongolia. *Earth Science (Journal of China University of Geosciences)* **35**, 933–46 (in Chinese with English abstract).

FURMAN, T. & GRAHAM, D. 1999. Erosion of lithospheric mantle beneath the East African Rift system: geochemical evidence from the Kivu volcanic province. *Lithos* **48**, 237–62.

GAO, S., LUO, T. G., ZHANG, B. R., ZHANG, H. F., HAN, Y. W., ZHAO, Z. D. & HU, Y. K. 1998. Chemical composition of the continental crust as revealed by studies in East China. *Geochimica et Cosmochimica Acta* **62**, 1959–75.

GAO, S., RUDNICK, R. L., CARLSON, R. W., MCDONOUGH, W. F. & LIU, Y. S. 2002. Re–Os evidence for replacement of ancient mantle lithosphere beneath the North China Craton. *Earth and Planetary Science Letters* **198**, 307–22.

GAO, S., RUDNICK, R. L., YUAN, H. L., LIU, X. M., LIU, Y. S., XU, W. L., LING, W. L., AYERS, J., WANG, X. C. & WANG, Q. H. 2004. Recycling lower continental crust in the North China Craton. *Nature* **432**, 892–7.

GOLDSTEIN, S. L., O'NIONS, R. K. & HAMILTON, P. J. 1984. A Sm–Nd isotopic study of atmospheric dusts and particulates from major river systems. *Earth and Planetary Science Letters* **70**, 221–36.

GRIFFIN, W. L., O'REILLY, S. Y. & RYAN, C. G. 1992. Composition and thermal structure of the lithosphere beneath South Africa, Siberia and China: proton microprobe studies. In *International Symposium on Cenozoic Volcanic Rocks and Deep-seated Xenoliths of China and Its Environs*, pp. **20**, 8–12 September 1992, Beijing.

GRIFFIN, W. L., ZHANG, A. D., O'REILLY, S. Y. & RYAN, C. G. 1998. Phanerozoic evolution of the lithosphere beneath the Sino-Korean Craton. In *Mantle Dynamics and Plate Internationals in East Asia* (eds M. Flower, S. L. Chung & C. H. Lo), pp. 107–26. American Geophysical Union, Geodynamics Series 27.

GUO, F., NAKAMURU, E., FAN, W. M., KOBAYOSHI, K. & LI, C. W. 2007. Generation of Palaeocene akakitic andesites by magma mixing; Yanji area, NE China. *Journal of Petrology* **48**, 661–92.

HAMILTON, P. J., O'NIONS, R. K., BRIDGWATER, D. & NUTMAN, A. 1983. Sm–Nd studies of Archaean metasediments and metavolcanics from West Greenland and their implications for the Earth's early history. *Earth and Planetary Science Letters* **62**, 263–72.

HAN, B. F., KAGAMI, H. & LI, H. M. 2004. Age and Nd–Sr isotopic geochemistry of the Guangtoushan alkaline granite, Hebei province, China: implications for Early Mesozoic crust-mantle interaction in North China Block. *Acta Petrologica Sinica* **20**, 1375–88 (in Chinese with English abstract).

HU, Z. C., LIU, Y. S., GAO, S., LIU, W. G., ZHANG, W., TONG, X. R., LIN, L., ZONG, K. Q., LI, M., CHEN, H. H., ZHOU, L. & YANG, L. 2012. Improved in situ Hf isotope ratio analysis of zircon using newly designed X skimmer cone and jet sample cone in combination with the addition of nitrogen by laser ablation multiple collector ICP-MS. *Journal of Analytical Atomic Spectrometry* **27**, 1391–9.

JAHN, B. M. & ZHANG, Z. Q. 1984. Archean granulite gneisses from eastern Hebei Province China: rare earth geochemistry and tectonic implications. *Contributions to Mineralogy and Petrology* **85**, 224–43.

JIANG, Y. H., JIANG, S. Y., LING, H. F. & NI, P. 2010. Petrogenesis and tectonic implications of Late Jurassic shoshonitic lamprophyre dikes from the Liaodong Peninsula, NE China. *Mineralogy and Petrology* **100**, 127–51.

JIN, W., LI, S. X. & LIU, X. S. 1991. The metamorphic dynamics of Early Precambrian high-grade metamorphic rocks series in Daqing-Ulashan area, Inner Mongolia. *Acta Petrlogica Sinica* **7**, 27–35 (in Chinese with English abstract).

KAY, R. W. 1978. Aleutian magnesian andesites: melts from subducted Pacific Ocean crust. *Journal of Volcanology and Geothermal Research* **4**, 117–32.

KELEMEN, P. D., DICK, H. J. B. & QUICK, J. E. 1992. Formation of harzburgite by pervasive melt/rock reaction in the upper mantle. *Nature* **358**, 635–41.

KLEMME, S. & O'NEILL, H. S. 2000. The near-solidus transition from garnet lherzolite to spinel lherzolite. *Contributions to Mineralogy and Petrology* **138**, 237–48.

KRÖNER, A., CUI, W. Y., WANG, S. Q., WANG, C. Q. & NEMCHIN, A. A. 1998. Single zircon ages from high-grade rocks of the Jianping complex, Liaoning Province, NE China. *Journal of Asian Earth Sciences* **16**, 519–32.

LI, J. Y. 2006. Permian geodynamic setting of Northeast China and adjacent regions: closure of the Paleo-Asian Ocean and subduction of the Paleo-Pacific Plate. *Journal of Asian Earth Sciences* **26**, 207–24.

LI, Q. L., WU, F. Y., LI, X. H., QIU, Z. L., LIU, Y., YANG, Y. H. & TANG, G. Q. 2011. Precisely dating Paleozoic kimberlites in the North China Craton and Hf isotopic constraints on the evolution of the subcontinental lithospheric mantle. *Lithos* **126**, 127–34.

LI, S. Z., ZHAO, G. C., SUN, M., HAN, Z. Z., LUO, Y., HAO, D. F. & XIA, X. P. 2005. Deformation history of the Paleoproterozoic Liaohe assemblage in the Eastern Block of the North China Craton. *Journal of Asian Earth Sciences* **24**, 659–74.

LIN, S. Z., ZHU, G., YAN, L. J., SONG, L. H. & LIU, B. 2013. Structural and chronological constraints on a Late Paleozoic shortening event in the Yanshan tectonic belt. *Chinese Science Bulletin* **58**, 3922–36 (in Chinese with English abstract).

LING, W. L., DUAN, R. C., XIE, X. J., ZHANG, Y. Q., ZHANG, J. B., CHENG, J. P., LIU, X. M. & YANG, H. M. 2009. Contrasting geochemistry of the Cretaceous volcanic suites in Shandong Province and its implications for the Mesozoic lower crust delamination in the eastern North China Craton. *Lithos* **133**, 640–58.

LIU, D. Y., NUTMAN, A. P., COMPSTON, W., WU, J. S. & SHEN, Q. H. 1992. Remnants of ≥3800 Ma crust in the Chinese part of the Sino-Korean Craton. *Geology* **20**, 339–42.

LIU, H. T., SUN, S. H., LIU, J. M. & ZHAI, M. G. 2002. The Mesozoic high-Sr granitoids in the northern marginal region of North China Craton: geochemistry and source region. *Acta Petrologica Sinica* **18**, 257–74 (in Chinese with English abstract).

LIU, J. G., CARLSON, R. W., RUDNICK, R. L., WALKER, R. J., GAO, S. & WU, F. Y. 2012. Comparative Sr-Nd-Hf-Os-Pb isotope systematics of xenolithic peridotites from Yangyuan, North China Craton: Additional evidence for a Paleoproterozoic age. *Chemical Geology* **332–3**, 1–14.

LIU, J. G., RUDNICK, R. L., WALKER, R. J., GAO, S., WU, F. Y., PICCOLI, P. M., YUAN, H. L., XU, W. L. & XU, Y. G. 2011. Mapping lithospheric boundaries using Os isotopes of mantle xenoliths: an example from the North China Craton. *Geochimica et Cosmochimica Acta* **75**, 3881–902.

LIU, J. G., RUDNICK, R. L., WALKER, R. J., XU, W. L., GAO, S. & WU, F. Y. 2015. Big insights from tiny peridotites: evidence for persistence of Precambrian lithosphere beneath the eastern North China Craton. *Tectonophysics* **650**, 104–12.

LIU, Y. S., GAO, S., HU, Z. C., GAO, C. G., ZONG, K. Q. & WANG, D. B. 2010a. Continental and oceanic crust recycling-induced melt-peridotite interactions in the Trans-North China Orogen: U–Pb dating, Hf isotopes and trace elements in zircons of mantle xenoliths. *Journal of Petrology* **51**, 537–71.

LIU, Y. S., GAO, S., YUAN, H. L., ZHOU, L., LIU, X. M., WANG, X. C., HU, Z. C. & WANG, L. S. 2004. U–Pb zircon ages and Nd, Sr and Pb isotopes of lower crustal xenoliths from North China Craton: insights on evolution of lower continental crust. *Chemical Geology* **211**, 87–109.

LIU, Y. S., HU, Z. C., GAO, S., GÜNTHER, D., XU, J., GAO, C. G. & CHEN, H. H. 2008. In situ analysis of major and trace elements of anhydrous minerals by LA-ICP-MS without applying an internal standard. *Chemical Geology* **257**, 34–43.

LIU, Y. S., HU, Z. C., ZONG, K. Q., GAO, C. G., GAO, S., XU, J. & CHEN, H. H. 2010b. Reappraisement and refinement of zircon U–Pb isotope and trace element analyses by LA-ICP-MS. *Chinese Science Bulletin* **55**, 1535–46.

LU, F. X., HAN, Z. G., ZHENG, J. P. & REN, Y. X. 1991. Characteristics of Paleozoic mantle-lithosphere in Fuxian, Liaoning Province. *Geological Science and Technology Information* **10**, 2–20 (in Chinese with English abstract).

LUDWIG, K. R. 2003. *User's Manual for ISOPLOT 3.00: A Geochronological Toolkit for Microsoft Excel*. Berkeley Geochronology Center, Special Publication no. 4.

LUO, Z. K., LI, J. J., GUAN, K., QIU, Y. S., QIU, Y. M., MCNAUGHTON, N. J. & GROVES, D. I. 2004. SHRIMP zircon U–Pb age of the granite at Baizhangzi gold field in Lingyuan, Liaoning province. *Geological Survey and Research* **27**, 82–5 (in Chinese with English abstract).

LUO, Z. K., MIAO, L. C., GUAN, K., QIU, Y. S. & QIU, Y. M. 2003. SHRIMP U–Pb zircon dating of the Dushan granitic batholiths and related granite-porphyry dyke, eastern Hebei Province, China, and their geological significance. *Geochimica* **32**, 173–80 (in Chinese with English abstract).

MA, L., JIANG, S. Y., HOFMANN, A. W., DAI, B. Z., HOU, M. L., ZHAO, K. D., CHEN, L. H., LI, J. W. & JIANG, Y. H. 2014a. Lithospheric and asthenospheric sources of lamprophyres in the Jiandong Peninsula: a consequence of rapid lithospheric thinning beneath the North China Craon? *Geochimica et Cosmochimica Acta* **124**, 250–71.

MA, L., JIANG, S. Y., HOU, M. L., DAI, B. Z., JIANG, Y. H., YANG, T., ZHAO, K. D., PU, W., ZHU, Z. Y. & XU, B.

2014b. Geochemistry of Early Cretaceous calc-alkaline lamprophyres in the Jiaodong Peninsula: implication for lithospheric evolution of the eastern North China Craton. *Gondwana Research* **25**, 859–72.

Ma, Q., Zheng, J. P., Griffin, W. L., Zhang, M., Tang, H. Y., Su, Y. P. & Ping, X. Q. 2012. Triassic "adakitic" rocks in an extensional setting (North China): melts from the cratonic lower crust. *Lithos* **149**, 159–73.

Ma, Q., Zheng, J. P., Xu, Y. G., Griffin, W. L. & Zhang, R. S. 2015. Are continental "adakites" derived from thickened or foundered lower crust? *Earth and Planetary Science Letters* **419**, 125–33.

Ma, X. Y. 1987. *Lithospheric Dynamics Map of China and Adjacent Seas (1:4,000,000) and Explanatory Notes*. Beijing: Geological Publishing House (in Chinese).

MacPherson, C. G., Dreher, S. T. & Thirlwall, M. F. 2006. Adakites without slab melting: high pressure differentiation of island arc magma, Mindanao, the Philippines. *Earth and Planetary Science Letters* **243**, 581–93.

Martin, H. 1999. Adakitic magmas: modern analogues of Archaean granitoids. *Lithos* **46**, 411–29.

Martin, H., Smithies, R. H., Rapp, R., Moyen, J. F. & Champion, D. 2005. An overview of adakite, tonalite-trondhjemite-granodiorite (TTG), and sanukitoid: relationships and some implications for crustal evolution. *Lithos* **79**, 1–24.

McCulloch, M. T., Rosman, K. J. R. & De Laeter, J. R. 1977. The isotopic and elemental abundance of ytterbium in meteorites and terrestrial samples. *Geochimica et Cosmochimica Acta* **41**, 1703–7.

McKenzie, D. P. 1989. Some remarks on the movement of small melt fractions in the mantle. *Earth and Planetary Science Letters* **95**, 53–72.

McKenzie, D. & O'Nions, R. K. 1991. Partial melt distributions from inversion of rare earth element concentrations. *Journal of Petrology* **32**, 1021–91.

Menzies, M. A., Fan, W. M. & Zhang, M. 1993. Palaeozoic and Cenozoic lithoprobes and the loss of >120 km of Archaean lithosphere, Sino-Korean Craton, China. In *Magmatic Processes and Plate Tectonic* (eds H. M. Prichard, T. Alabaster, N. B. W. Harris & C. R. Neary), pp. 71–81. Geological Society of London, Special Publication no. 76.

Menzies, M. A. & Xu, Y. G. 1998. Geodynamics of the North China Craton. In *Mantle Dynamics and Plate Internationals in East Asia* (eds M. Flower, S. L. Chung & C. H. Lo), pp. 155–65. American Geophysical Union, Geodynamics Series 27.

Menzies, M. A., Xu, Y. G., Zhang, H. F. & Fan, W. M. 2007. Integration of geology, geophysics and geochemistry: a key to understanding the North China Craton. *Lithos* **96**, 1–21.

Miao, L. C., Luo, Z. K., Guan, K. & Huang, J. Z. 1998. The implication of the SHRIMP U–Pb age in zircon to the petrogenesis of the Linglong granite, east Shangdong Province. *Acta Petrologica Sinica* **14**, 198–206 (in Chinese with English abstract).

Mu, B. L., Shao, J. A., Chu, Z. Y., Yan, G. H. & Qiao, G. S. 2001. Sm–Nd age and Sr, Nd isotopic characteristics of the Fanshan potassic alkaline ultramafic-syenite complex in Hebei province, China. *Acta Petrologica Sinica* **17**, 358–65 (in Chinese with English abstract).

Niu, Y. L. 2005. Generation and evolution of basaltic magmas: some basic concepts and a new view on the origin of Mesozoic-Cenozoic basaltic volcanism in eastern China. *Geological Journal of China Universities* **11**, 9–46.

Pei, F. P., Xu, W. L., Yu, Y., Zhao, Q. G. & Yang, D. B. 2008. Petrogenesis of the Late Triassic Mayihe pluton in southern Jilin Province: evidence from zircon U–Pb geochronology and geochemistry. *Earth Science Edition (Journal of Jilin University)* **38**, 351–62 (in Chinese with English abstract).

Peng, P., Zhai, M. G., Guo, J. H., Zhang, H. F. & Zhang, Y. B. 2008. Petrogenesis of Tiassic post-collisional syenite plutons in the Sino-Korean Craton: an example from North Korea. *Geological Magazine* **145**, 637–47.

Peucat, J. J., Vidal, P., Bernard-Griffiths, J. & Condie, K. C. 1989. Sr, Nd, and Pb isotopic systematics in the Archean low- to high-grade transition zone of Southern India: syn-accretion vs. post-accretion granulites. *The Journal of Geology* **97**, 537–49.

Pidgeon, R. T. 1980. Isotopic ages of the zircons from the Archean granulite facies rocks, Eastern Hebei, China. *Geological Review* **26**, 198–207.

Qian, Q. & Hermann, J. 2013. Partial melting of lower crust at 10–15 kbar: constraints on adakite and TTG formation. *Contributions to Mineralogy and Petrology* **165**, 1195–224.

Richards, J. P. & Kerrich, R. 2007. Special paper: adakite-like rocks: their diverse origins and questionable role in metallogenesis. *Economic Geology* **102**, 537–76.

Roberts, M. P. & Clemens, J. D. 1993. Origin of high-potassium, calc-alkaline, I-type granitoids. *Geology* **21**, 825–8.

Robinson, J. A. C. & Wood, B. J. 1998. The depth of the spinel to garnet transition at the peridotite solidus. *Earth and Planetary Science Letters* **164**, 277–84.

Rudnick, R. L. & Gao, S. 2003. The composition of the continental crust. In *The Crust* (eds R. L. Rudnick), pp. 1–64. Oxford: Elsevier-Pergamon.

Rudnick, R. L. & Gao, S. 2014. Composition of the continental crust. In *Treatise on Geochemistry*, 2nd edition (eds H. D. Heinrich & K. K. Turekian), vol. 4, pp. 1–51. Oxford: Elsevier.

Salters, V. J. M. & Stracke, A. 2004. Composition of the depleted mantle. *Geochemistry, Geophysics, Geosystems* **5**, published online 13 May 2004, doi: 10.1029/2003GC000597.

Schiano, P., Clocchiatti, R., Shimizu, N., Maury, R. C., Jochum, K. P. & Hofmann, A. W. 1995. Hydrous, silica-rich melts in the sub-arc mantle and their relationship with erupted arc lavas. *Nature* **377**, 595–600.

Shao, J. A., Chen, F. K., Lu, F. X. & Zhou, X. H. 2006. Mesozoic pulsative upwelling diapirs of asthenosphere in west Liaoning Province. *Earth Science (Journal of China University of Geosciences)* **31**, 807–16 (in Chinese with English abstract).

Shao, J. A., Han, Q. J. & Li, H. M. 2000. Discovery of the Early Mesozoic granulite xenoliths in North China Craton. *Science in China (Series D)* **30**, 148–53 (in Chinese).

Shao, J. A., Han, Q. J., Zhang, L. Q. & Mou, B. L. 1999. Discovery of Early Mesozoic cumulate complex xenoliths in eastern Inner Mongolia. *Chinese Science Bulletin* **44**, 478–85 (in Chinese).

Shao, J. A. & Zhang, L. Q. 2002. Mesozoic dyke swarms in the north of North China. *Acta Petrologica Sinica*, **18**, 312–8 (in Chinese with English abstract).

Shao, J. A., Zhang, L. Q. & Li, D. M. 2002. Three Proterozoic extensional events in North China Craton. *Acta Petrologica Sinica* **18**, 152–60 (in Chinese with English abstract).

She, H. Q., Wang, Y. W., Li, Q. H., Zhang, D. Q., Feng, C. Y. & Li, D. X. 2006. The mafic granulite xenoliths and its implications to mineralization in Chaihulanzi gold deposit, Inner Mongolian, China. *Acta Geologica Sinica* **80**, 863–75 (in Chinese with English abstract).

SONG, B., NUTMAN, A. P., LIU, D. Y. & WU, J. S. 1996. 3800 to 2500 Ma crustal evolution in Anshan area of Liaoning Province, Northeastern China. *Precambrian Research* **78**, 79–94.

STERN, R. A. & HANSON, G. N. 1991. Archean high-Mg granodiorite: a derivative of light rare earth element-enriched monzodiorite of mantle origin. *Journal of Petrology* **32**, 201–38.

STRECK, M. J., LEEMAN, W. P. & CHESLEY, J. 2007. High-magnesian andesite from Mount Shasta: a product of magma mixing and contamination, not a primitive mantle melt. *Geology* **35**, 351–4.

SUN, S. S. & MCDONOUGH, W. F. 1989. Chemical and isotopic systematics of oceanic basalts: implications for mantle composition and processes. In *Magmatism in Ocean Basins* (eds A. D. Saunders & M. J. Norry), pp. 313–45. Geological Society of London, Special Publication no. 42.

TIAN, W., CHEN, B., LIU, C. Q. & ZHANG, H. F. 2007. Zircon U–Pb age and Hf isotopic composition of the Xiaozhangjiakou ultramafic pluton in northern Hebei. *Acta Petrologica Sinica* **23**, 583–90 (in Chinese with English abstract).

WANG, F., CHEN, F. K., HOU, Z. H., PENG, P. & ZHAI, M. G. 2009. Zircon ages and Sr–Nd–Hf isotopic composition of Late Paleozoic granitoids in the Chongli-Chicheng area, northern margin of the North China Block. *Acta Petrologica Sinica* **25**, 3057–74 (in Chinese with English abstract).

WANG, Q., WYMAN, D. A., XU, J. F., JIAN, P., ZHAO, Z. H., LI, C. F., XU, W., MA, J. L. & HE, B. 2007. Early Cretaceous adakitic granites in the Northern Dabie Complex, central China: implications for partial melting and delamination of thickened lower crust. *Geochimica et Cosmochimica Acta* **71**, 2609–36.

WINDLEY, B. F., ALEXEIEV, D., XIAO, W. J., KRÖNER, A. & BADARCH, G. 2007. Tectonic models for accretion of the Central Asian Orogenic Belt. *Journal of the Geological Society* **164**, 31–47.

WINTHER, K. T. 1996. An experimentally based model for the origin of tonalitic and trondhjemitic melts. *Chemical Geology* **127**, 43–59.

WU, C. H. & ZHONG, C. T. 1998. Early Proterozoic SW-NE collision model for the central part of the North China Craton: implications for tectonic regime of the khondalite downward into lower crust in Jin-Meng high-grade region. *Progress in Precambrian Research* **21**, 28–50 (in Chinese with English abstract).

WU, F. Y., JAHN, B. M. & LIN, Q. 1997. Isotopic characteristics of post-orogenic granites in North China orogen and its implications for crust growth. *Chinese Science Bulletin* **42**, 2188–92 (in Chinese).

WU, F. Y., SUN, D. Y., GE, W. C., ZHANG, Y. B., GRANT, M. L., WILDE, S. A. & JAHN, B. M. 2011. Geochronology of the Phanerozoic granitoids in northeastern China. *Journal of Asian Earth Sciences* **41**, 1–30.

WU, F. Y., WALKER, R. J., YANG, Y. H., YUAN, H. L. & YANG, J. H. 2006*a*. The chemical-temporal evolution of lithospheric mantle underlying the North China Craton. *Geochimica et Cosmochimica Acta* **70**, 5013–34.

WU, F. Y., WILDE, S. A., ZHANG, G. L. & SUN, D. Y. 2004. Geochronology and petrogenesis of the post-orogenic Cu-Ni sulfide-bearing mafic-ultramafic complexes in Jilin Province, NE China. *Journal of Asian Earth Sciences* **23**, 781–97.

WU, F. Y., XU, Y. G., GAO, S. & ZHENG, J. P. 2008. Lithospheric thinning and destruction of the North China Craton. *Acta Petrologica Sinica* **24**, 1145–74 (in Chinese with English abstract).

WU, F. Y., YANG, J. H. & LIU, X. M. 2005. Geochronological framework of the Mesozoic granitic magmatism in the Liaodong Peninsula, Northeast China. *Geological Journal of China Universities* **11**, 305–17 (in Chinese with English abstract).

WU, F. Y., YANG, J. H., ZHANG, Y. B. & LIU, X. M. 2006*b*. Emplacement ages of the Mesozoic granites in southeastern part of the western Liaoning Province. *Acta Petrologica Sinica* **22**, 315–25 (in Chinese with English abstract).

WU, J. S., GENG, Y. S., SHEN, Q. H., LIU, D. Y., LI, Z. L. & ZHAO, D. M. 1991. *The Early Precambrian Significant Geological Events in the North China Craton*. Beijing: Geological Publishing House, pp. 1–115 (in Chinese with English abstract).

WU, M. Q., ZHAO, G. C., GAO, J. W. & WANG, H. T. 2014. Geochemical characteristics of the Dushan complex and their geological significance. *Geology in China* **41**, 108–21 (in Chinese with English abstract).

XIA, Q. K., LIU, J., LIU, S. C., KOVÁCS, I., FENG, M. & DANG, L. 2013. High water content in Mesozoic primitive basalts of the North China Craton and implications on the destruction of cratonic mantle lithosphere. *Earth and Planetary Science Letters* **361**, 85–97.

XIAO, W. J., WINDLEY, B. F., HAO, J. & ZHAI, M. G. 2003. Accretion leading to collision and the Permian Solonker suture, Inner Mongolia, China: termination of the central Asian orogenic belt. *Tectonics* **22**, 1484–505.

XIAO, W. J., WINDLEY, B. F., HUANG, B. C., HAN, C. M., YUAN, C., CHEN, H. L., SUN, M., SUN, S. & LI, J. L. 2009. End-Permian to mid-Triassic termination of the accretionary processes of the southern Altaids: implications for the geodynamic evolution, Phanerozoic continental growth, and metallogeny of Central Asia. *International Journal of Earth Sciences* **98**, 1189–17.

XIONG, L., SHI, W. J., LI, H., TIAN, N., CHEN, C., ZHOU, H. Z., ZHAO, S. Q. & LI, P. Y. 2017. Geochemistry, Sr-Nd-Hf isotopes and petrogenesis of Mid-Late Triassic Baizhangzi granitic intrusive rocks in eastern Hebei-western Liaoning Province. *Earth Science (Journal of China University of Geosciences)* **42**, 207–22 (in Chinese with English abstract).

XU, J. F., SHINJO, R., DEFANT, M. J., WANG, Q. & RAPP, R. P. 2002. Origin of Mesozoic adakitic intrusive rocks in the Ningzhen area of east China: partial melting of delaminated lower continental crust. *Geology* **30**, 1111–4.

XU, W. L., PEI, F. P., WANG, F., MENG, E., JI, W. Q., YANG, D. B. & WANG, W. 2013. Spatial-temporal relationships of Mesozoic volcanic rocks in NE China: constraints on tectonic overprinting and transformations between multiple tectonic regimes. *Journal of Asian Earth Sciences* **74**, 167–93.

XU, W. L., WANG, Q. H., WANG, D. Y., GUO, J. H. & PEI, F. P. 2006a. Mesozoic adakitic rocks from the Xuzhou-Suzhou area, eastern China: evidence for partial melting of delaminated lower continental crust. *Journal of Asian Earth Sciences* **27**, 454–64.

XU, W. L., YANG, C. H., YANG, D. B., PEI, F. P., WANG, Q. H. & JI, W. Q. 2006b. Mesozoic high Mg diorites in eastern North China Craton: constraints on the mechanism of lithospheric thinning. *Earth Science Frontiers* **13**, 120–9 (in Chinese with English abstract).

XU, X., O'REILLY, S. Y., GRIFFIN, W. L. & ZHOU, X. 1998. The nature of the Cenozoic lithosphere at Nushan, eastern China. In *Mantle Dynamics and Plate Interactions in East Asia* (eds M. Flower, S. L. Chung, C. H. Lo & Y. Y. Lee), pp. 167–96. American Geophysical Union, Geodynamics Series 27.

XU, Y. G. 2001. Thermo-tectonic destruction of the Archaean lithospheric keel beneath the Sino-Korean Craton in China: evidence, timing and mechanism. *Physics and Chemistry of the Earth* **26**, 747–57.

XU, Y. G. 2006. Using basalt geochemistry to constrain Mesozoic-Cenozoic evolution of the lithosphere beneath North China Craton. *Earth Science Frontiers* **13**, 93–104 (in Chinese with English abstract).

XU, Y. G., HUANG, X. L., MA, J. L., WANG, Y. B., IIZUKA, Y., XU, J. F., WANG, Q. & WU, X. Y. 2004. Crust-mantle interaction during the tectono-thermal reactivation of the North China Craton: constraints from SHRIMP zircon U–Pb chronology and geochemistry of Mesozoic plutons from western Shandong. *Contributions to Mineralogy and Petrology* **147**, 750–67.

XU, Y. G., LI, H. Y., PANG, C. J. & HE, B. 2009. On the timing and duration of the destruction of the North China Craton. *Chinese Science Bulletin* **54**, 3379–96.

YAN, G. H., MOU, B. L., XU, B. L., HE, G. Q., TAN, L. K., ZHAO, H., HE, Z. F., ZHANG, R. H. & QIAO, G. S. 2000. Triassic alkaline intrusive in the Yanliao-Yinshan area: chronology, Sr, Nd and Pb isotopic characteristics and their implication. *Science in China (Series D)* **30**, 383–7 (in Chinese).

YANG, J. H., SUN, J. F., ZHANG, M., WU, F. Y. & WILDE, S. A. 2012. Petrogenesis of silica-saturated and silica-undersaturated syenites in the northern North China Craton related to post-collisional and intraplate extension. *Chemical Geology* **328**, 149–67.

YANG, J. H., WU, F. Y., WILDE, S. A. & LIU, X. M. 2007. Petrogenesis of Late Triassic granitoids and their enclaves with implications for post-collisional lithospheric thinning of the Liaodong Peninsula, North China Craton. *Chemical Geology* **242**, 155–75.

YE, H., ZHANG, S. H., ZHAO, Y. & WU, F. 2014. Petrogenesis and emplacement deformation of the Late Triassic Dushan composite botholith in the Yanshan fold and thrust belt: implications for the tectonic settings of the northern margin of the North China Craton during the Early Mesozoic. *Earth Science Frontiers* **21**, 275–92 (in Chinese with English abstract).

ZHAI, M. G. & SANTOSH, M. 2011. The Early Precambrian odyssey of the North China Craton: a synoptic overview. *Gondwana Research* **20**, 6–25.

ZHANG, C. H., LI, C. M., DENG, H. L., LIU, Y., LIU, L., WEI, B., LI, H. B. & LIU, Z. 2011. Mesozoic contraction deformation in the Yanshan and northern Taihang mountains and its implications to the destruction of the North China Craton. *Science in China (Series D)* **54**, 798–822.

ZHANG, H. F., GOLDSTEIN, S. L., ZHOU, X. H., SUN, M., ZHENG, J. P. & CAI, Y. 2008. Evolution of subcontinental lithospheric mantle beneath eastern China: Re-Os isotopic evidence from mantle xenoliths in Paleozoic kimberlites and Mesozoic basalts. *Contributions to Mineralogy and Petrology* **155**, 271–93.

ZHANG, H. F., SUM, M., ZHOU, X. H., FAN, W. M., ZHAI, M. G. & YIN, J. F. 2002. Mesozoic lithosphere destruction beneath the North China craton: evidence from major-, trace-element and Sr–Nd–Pb isotope studies of Fangcheng basalts. *Contributions to Mineralogy and Petrology* **144**, 241–53.

ZHANG, S. H., ZHAO, Y., LIU, J. M., HU, J. M., SONG, B. & WU, H. 2010a. Geochronology, geochemistry and tectonic setting of the Late Paleozoic-Early Mesozoic magmatism in the northern margin of the North China Block: a preliminary review. *Acta Petrologica et Mineralogica* **29**, 824–42 (in Chinese with English abstract).

ZHANG, S. H., ZHAO, Y., LIU, X. H., LIU, D. Y., CHEN, F. K., XIE, L. W. & CHEN, H. H. 2009a. Late Paleozoic to Early Mesozoic mafic-ultramafic complexes from the northern North China Block: constraints on the composition and evolution of the lithospheric mantle. *Lithos* **110**, 229–46.

ZHANG, X. H., YUAN, L. L. & WILDE, S. A. 2014. Crust/mantle interaction during the construction of an extensional magmatic dome: Middle to Late Jurassic plutonic complex from western Liaoning, North China Craton. *Lithos* **205**, 185–207.

ZHANG, X. H., ZHANG, H. F., JIANG, N. & WILDE, S. A. 2010*b*. Contrasting Middle Jurassic and Early Cretaceous mafic intrusive rocks from western Liaoning, North China Craton: petrogenesis and tectonic implications. *Geological Magazine* **147**, 844–59.

ZHANG, S. H., ZHAO, Y., SONG, B., HU, J. M., LIU, S. W., YANG, Y. H., CHEN, F. K., LIU, X. M. & LIU, J. 2009b. Contrasting Late Carboniferous and Late Permian-Middle Triassic intrusive suites from the northern margin of the North China Craton: geochronology, petrogenesis, and tectonic implications. *Geological Society of America Bulletin* **121**, 181–200.

ZHANG, S. H., ZHAO, Y., YE, H., HOU, K. J. & LI, C. F. 2012. Early Mesozoic alkaline complexes in the northern North China Craton: implications for cratonic lithospheric destruction. *Lithos* **155**, 1–18.

ZHAO, G. C., SUN, M., WILDE, S. A. & ZHONG, L. S. 2005. Late Archean to Paleoproterozoic evolution of the North China Craton: key issues revisited. *Precambrian Research* **136**, 177–202.

ZHAO, G. C., WILDE, S. A., CAWOOD, P. A. & SUN, M. 2001. Archean blocks and their boundaries in the North China Craton: lithological, geochemical, structural and P–T path constraints and tectonic evolution. *Precambrian Research* **107**, 45–73.

ZHENG, J. P., GRIFFIN, W. L., MA, Q., O'REILLY, S. Y., XIONG, Q., TANG, H. Y., ZHAO, J. H., YU, C. M. & SU, Y. P. 2012. Accretion and reworking beneath the North China Craton. *Lithos* **149**, 61–78.

ZHENG, J. P., GRIFFIN, W. L., O'REILLY, S. Y., LU, F. X., YU, C. M., ZHANG, M. & LI, H. M. 2004a. U–Pb and Hf-isotope analysis of zircons in mafic xenoliths from Fuxian kimberlites: evolution of the lower crust beneath the North China craton. *Contributions to Mineralogy and Petrology* **148**, 79–103.

ZHENG, J. P. & LU, F. X. 1999. Mantle xenoliths from kimberlites, Shandong and Liaoning Paleozoic mantle character and its heterogeneity. *Acta Petrologica Sinica* **15**, 65–74 (in Chinese with English abstract).

ZHENG, J. P., PING, X. Q., XIA, B. & YU, C. M. 2013. The weak Neoproterozoic thermal records in North China and its significances for the lithospheric thickness. *Acta Petrologica Sinica* **29**, 2456–64 (in Chinese with English abstract).

ZHENG, J. P., YU, C. M., LU, F. X. & LI, H. M. 2004b. Geochemical and geochronological characteristics of metabasaltic xenoliths: implications for the evolution of continental lower crust in early time. *Science in China (Series D)* **34**, 412–22 (in Chinese with English abstract).

ZHU, R. X., YANG, J. H. & WU, F. Y. 2012. Timing of destruction of the North China Craton. *Lithos* **149**, 51–60.